

Review

# SPIONs Magnetophoresis and Separation via Permanent Magnets: Biomedical and Environmental Applications

Xian Wu <sup>1,†</sup>, Stefano Ciannella <sup>2,†</sup> , Hyeon Choe <sup>1</sup>, Jacob Strayer <sup>1</sup> , Kai Wu <sup>3</sup> , Jeffrey Chalmers <sup>1</sup>   
and Jenifer Gomez-Pastora <sup>2,\*</sup> 

- <sup>1</sup> William G. Lowrie Department of Chemical and Biomolecular Engineering, The Ohio State University, 151 West Woodruff Avenue, Columbus, OH 43210, USA; wu.4073@buckeyemail.osu.edu (X.W.); choe.123@buckeyemail.osu.edu (H.C.); strayer.117@buckeyemail.osu.edu (J.S.); chalmers.1@osu.edu (J.C.)
- <sup>2</sup> Department of Chemical Engineering, Texas Tech University, 2500 Broadway, Lubbock, TX 79409, USA; stefano.ciannella@ttu.edu
- <sup>3</sup> Department of Electrical and Computer Engineering, Texas Tech University, 2500 Broadway, Lubbock, TX 79409, USA; kai.wu@ttu.edu
- \* Correspondence: jenifer.gomez@ttu.edu; Tel.: +1-(806)-742-3553
- † These authors contributed equally to this work.

**Abstract:** Superparamagnetic iron oxide nanoparticles (SPIONs) have emerged as cutting-edge materials, garnering increasing attention in recent years within the fields of chemical and biomedical engineering. This increasing interest is primarily attributed to the distinctive chemical and physical properties of SPIONs. Progress in nanotechnology and particle synthesis methodologies has facilitated the fabrication of SPIONs with precise control over parameters such as composition, size, shape, stability, and magnetic response. Notably, these functionalized materials exhibit a remarkable surface-area-to-volume ratio, biocompatibility, and, most importantly, they can be effectively manipulated using external magnetic fields. Due to these exceptional properties, SPIONs have found widespread utility in the medical field for targeted drug delivery and cell separation, as well as in the chemical engineering field, particularly in wastewater treatment. Magnetic separation techniques driven by magnetophoresis have proven to be highly efficient, encompassing both high-gradient magnetic separation (HGMS) and low-gradient magnetic separation (LGMS). This review aims to provide an in-depth exploration of magnetic gradient separation techniques, alongside a comprehensive discussion of the applications of SPIONs in the context of drug delivery, cell separation, and environmental remediation.

**Keywords:** SPIONs; magnetophoresis; magnetic separation; drug delivery; cell separation; environmental remediation



**Citation:** Wu, X.; Ciannella, S.; Choe, H.; Strayer, J.; Wu, K.; Chalmers, J.; Gomez-Pastora, J. SPIONs Magnetophoresis and Separation via Permanent Magnets: Biomedical and Environmental Applications. *Processes* **2023**, *11*, 3316. <https://doi.org/10.3390/pr11123316>

Academic Editor: Fabio Carniato

Received: 1 November 2023

Revised: 22 November 2023

Accepted: 23 November 2023

Published: 28 November 2023



**Copyright:** © 2023 by the authors. Licensee MDPI, Basel, Switzerland. This article is an open access article distributed under the terms and conditions of the Creative Commons Attribution (CC BY) license (<https://creativecommons.org/licenses/by/4.0/>).

## 1. Introduction

In recent years, nanotechnology has gained considerable attention, leading to extensive research on nanomaterials and their diverse applications. Among the various types of nanomaterials, nanoparticles have emerged as a primary focus of investigation. These nanoparticles consist of particulate substances with dimensions of less than 100 nm [1]. One of the key factors driving this interest in nanoparticles is their exceptional properties arising from their diminutive size. As the dimensions of nanoparticles decrease, their surface-to-volume ratio increases, leading to enhanced particle performance. Notably, this larger surface-to-volume ratio imparts greater reactivity to the particles, resulting in higher fractions of reactive atoms on their surfaces compared to micro-particles or bulk materials [2]. Furthermore, due to their ideal surface properties, nanoparticles present an excellent opportunity for functionalization with diverse ligands, rendering them highly suitable candidates for the development of functional nanostructures. These unique characteristics have sparked significant scientific curiosity and motivated exploration into the potential applications of nanoparticles across various fields including bio-medical applications.

Among the diverse array of nanoparticles, magnetic nanoparticles (MNPs) stand out as one of the most extensively utilized materials owing to their unique magnetic properties [3]. For example, they can be used for targeted drug delivery [4], hyperthermia treatment [5], and magnetic resonance imaging (MRI) [6]. Typically, among MNPs, superparamagnetic iron oxide nanoparticles (SPIONs) have attracted increasing attention in the last few decades. SPIONs are single-domain nanoparticles that are usually composed of an iron oxide magnetic core (single-core), such as magnetite ( $\text{Fe}_3\text{O}_4$ ) or maghemite ( $\gamma\text{-Fe}_2\text{O}_3$ ), with a biocompatible polymer coating [7]. Multiple-core composites can also be synthesized with several magnetic cores per particle [6]. The distinctive magnetic characteristics of SPIONs stem from their iron oxide core, which confers superparamagnetism. This means that SPIONs exhibit high magnetization solely in the presence of a magnetic field and do not retain any magnetic moment once the magnetic field is removed [8]. The concept of superparamagnetism of magnetic nanomaterials was first proposed by Frenkel et al. in 1930 [9]. Since then, a variety of SPIONs have been developed for different applications. Moreover, the coatings serve the crucial purpose of preventing SPION aggregation and interactions with the surrounding environment, and their selection is typically dictated by the specific application requirements. By employing appropriate coatings, SPIONs become stable against oxidation and corrosion, and, notably, they exhibit enhanced physicochemical stability. Various types of coatings are employed for this purpose, encompassing both organic and inorganic materials. Among the organic coatings, surfactants, polymers, and activated carbon are commonly utilized. Meanwhile, inorganic components may also be employed in certain scenarios to achieve the desired protective and functional properties for the SPIONs. The choice of coating plays a pivotal role in optimizing the performance and effectiveness of SPIONs in diverse applications [10]. Ultimately, the surface coating offers the opportunity for attaching multiple ligands and surface groups, thereby enabling a wide range of applications [11].

Furthermore, the advantageous application potential of SPIONs has sparked significant interest in exploring the manipulation of these particles using magnetic field gradients, known as magnetophoresis, across various research fields [12]. The underlying principle of magnetic separation is predicated on exploiting the magnetic response of suspended particles to effectively remove them from mixtures employing inhomogeneous magnetic fields [13]. The magnetic properties of SPIONs facilitate their directed movement towards an external magnetic field gradient, enabling an efficient separation from the surrounding medium. The integration of SPIONs in numerous biomedical applications, such as bioseparation, typically involves a series of sequential steps: (1) conjugating the SPIONs to the target entities; (2) isolating the magnetically labeled target entities through magnetic separation techniques; and (3) conducting a subsequent analysis of the enriched target entities [14]. This study primarily focuses on the utilization of SPIONs manipulated with permanent magnets. However, it is noteworthy that SPIONs can alternatively be controlled by employing electromagnets [15]. Magnetically actuated systems with electromagnets have been devised among others for drug delivery applications to enhance drug absorption [15]. For instance, Gong et al. introduced an innovative approach employing magnetic biohybrid microrobot multimers (BMMs) that integrated electromagnets for precise and targeted drug delivery [16]. Moreover, Li et al. focused on the development and application of pH-responsive theranostic nanoplatforms containing SPIONs to enhance cancer diagnosis and treatment by achieving targeted delivery of therapeutic agents to pathological tissues [17].

The utilization of magnetic separation offers several advantages for manipulating SPIONs when compared to conventional methods employed for separating small solids from liquids, such as sedimentation and filtration [18]. Firstly, magnetic separation exhibits a potential increase in efficiency over conventional processes, enabling the effective separation of magnetic materials from nonmagnetic solids. This specificity allows for more precise and targeted separations. Secondly, magnetic separation generally outperforms conventional methods in terms of speed, as the applied flow rate can be substantially higher,

reaching two orders of magnitude greater than ordinary filtration [19]. This enhanced velocity facilitates a faster processing of samples, reducing separation time. Additionally, magnetic separation presents economic benefits due to its relatively compact space requirements. It does not demand large equipment or installations, making it a cost-effective and space-efficient approach. Moreover, magnetic separation is not sensitive to environmental factors such as pH or temperature [20]. This robustness enables its operation across a wider range of pH levels and temperatures, rendering it versatile and adaptable for diverse experimental conditions. Furthermore, SPIONs exhibit lower toxicity and enhanced biocompatibility compared to other metallic nanoparticle counterparts, rendering them promising candidates for environmental remediation as well as for several bioapplications [21,22]. Importantly, magnetic remediation involving SPIONs is characterized by its reliability, and these nanoparticles can be effectively recycled for subsequent applications with consistently high efficiency, which decreases process costs [23].

In this work, we offer a comprehensive and thorough study of the available magnetic field gradient separation methodologies, including high-gradient magnetic separation (HGMS) and low-gradient magnetic separation (LGMS), while also elucidating the fundamental principles of magnetophoresis and magnetic separation. Furthermore, we endeavor to engage in a comprehensive discourse regarding the diverse applications of SPIONs within the realms of drug delivery, cell separation, and environmental remediation.

## 2. Principles of Magnetophoresis/Magnetic Separation

Magnetic separation is a multifaceted process governed by various forces that dictate the behavior of materials under the influence of an external magnetic field. These forces encompass the magnetic force ( $\vec{F}_m$ ), gravity force ( $\vec{F}_g$ ), viscous drag ( $\vec{F}_d$ ), buoyancy, inertia, particle–fluid interactions, Brownian motion, as well as inter-particle phenomena including magnetic dipole interactions and Van der Waals forces [24]. The magnetic characteristics of SPIONs are contingent upon their specific composition [25]. When exposed to a magnetic field, the electron spins within the nanoparticles undergo rearrangement, resulting in the generation of magnetic dipole moments [26]. The magnetic properties of these particles can be effectively characterized by their magnetic susceptibility ( $\chi$ ) or magnetic permeability ( $\mu$ ).

The magnetic force acting on a particle is governed by its magnetization vector ( $\vec{M}$ , A/m), which arises due to the influence of an applied magnetic field. The magnetic susceptibility, as expressed by Equation (1), is the ratio of the induced magnetization in the particle to the strength of the external magnetic field ( $\vec{H}$ , A/m), and it is expressed as follows:

$$\chi = \frac{\vec{M}}{\vec{H}} \quad (1)$$

On the other hand, the magnetic permeability  $\mu$  is defined as the ratio of the magnetic flux density ( $\vec{B}$ , T) induced within the particle to the magnetic field strength ( $\vec{H}$ ). This parameter reflects the ease with which the magnetic field can permeate through the material, and it is mathematically represented as follows:

$$\mu = \frac{\vec{B}}{\vec{H}} \quad (2)$$

The magnetization vector  $\vec{M}$  represents the material's reaction to an applied external magnetic field strength  $\vec{H}$ . Consequently, the magnetic flux density vector  $\vec{B}$  can be

regarded as a superposition of the applied magnetic field and the material's magnetization response. The relationship among these parameters is defined as in the following expression:

$$\vec{B} = \mu_0 (\vec{H} + \vec{M}) \quad (3)$$

where  $\mu_0$  is the magnetic permeability of free space ( $4\pi \times 10^{-7}$  T/m). If the media are linear, homogenous, and isotropic, the vector quantities  $\vec{B}$ ,  $\vec{H}$ , and  $\vec{M}$  are proportional to each other, and Equation (3) can be expressed as follows [27]:

$$\vec{B} = \mu_0 (\vec{H} + \vec{M}) = \mu_0 (1 + \chi) \vec{H} = \mu \vec{H} \quad (4)$$

where

$$\mu = \mu_0 \mu_r = \mu_0 (1 + \chi) \quad (5)$$

Finally, the magnetic motion of the material can be calculated using the relative permeability ( $\mu_r$ ), defined as follows:

$$\mu_r = 1 + \chi \quad (6)$$

In the context of numerous applications, particles are often dispersed in aqueous solutions. In such scenarios, the magnetic force acting on the particle can be influenced by its assumed spherical shape and magnetization characteristics [28]. The expression for this magnetic force is as follows:

$$\vec{F}_m = 4\pi r_p^3 \frac{\mu_{r,p} - \mu_{r,f}}{\mu_{r,p} + 2\mu_{r,f}} \mu_{r,f} (\vec{H} \cdot \nabla \vec{B}) \quad (7)$$

where  $r_p$  (m) represents the radius of the particle and  $\mu_{r,p}$  and  $\mu_{r,f}$  are the relative permeabilities of the particles and the surrounding fluid, respectively. As indicated above, the magnetic field can be expressed as  $\vec{B} = (\mu_0 \mu_{r,f}) \vec{H}$ , leading to the formulation of Equation (8):

$$\vec{F}_m = 4\pi r_p^3 \frac{\chi_p - \chi_f}{\chi_p + 2\chi_f + 3} \left( \frac{\vec{B} \cdot \nabla \vec{B}}{\mu_0} \right) \quad (8)$$

where  $\chi_p$  and  $\chi_f$  are the susceptibilities of the particle and the surrounding fluid, respectively. The predominant opposing force vector to the magnetic force acting on a SPION is the fluid drag force  $\vec{F}_d$ , commonly estimated using Stokes' approximation for the viscous drag experienced by a sphere, as follows:

$$\vec{F}_d = 6\pi\eta r_p (\vec{v}_f - \vec{v}_p) \quad (9)$$

where  $\eta$  (Pa·s) is the kinematic viscosity of the fluid, and  $\vec{v}_f$  and  $\vec{v}_p$  are the velocity vectors of the fluid and the particle, respectively. To address this force, magnetophoresis models typically incorporate the fluid velocity field, which is governed by the Navier–Stokes and continuity equations for a non-compressible fluid and negligible gravitational force (i.e.,  $\rho \vec{g} \approx 0$ ):

$$\rho \left[ \frac{\partial \vec{v}}{\partial t} + (\vec{v} \cdot \nabla) \vec{v} \right] = -\nabla P + \eta \nabla^2 \vec{v} \quad (10)$$

$$\nabla \cdot \vec{v} = 0 \quad (11)$$

where  $\rho$  ( $\text{kg}/\text{m}^3$ ) represents the density of the fluid and  $P$  (Pa) is the pressure. The Navier–Stokes equation provides a mathematical description of the fluid flow dynamics, essential for understanding the magnetophoretic behavior of the SPIONs.

Additionally, the separation process must consider other cooperative effects. One such phenomenon is cooperative magnetophoresis, wherein particles tend to agglomerate. It can significantly accelerate the separation of SPIONs even under the influence of a low magnetic field gradient. Specifically, under the influence of an external magnetic field, the particles can aggregate, and as the aggregate reaches a critical size, the combined action of magnetic and gravitational forces can overcome thermal energy, leading to their collection [29]. This effect primarily arises from the particle–particle interactions [30] and can be described using the parameter  $\Psi$ , representing the ratio between the dipole–dipole contact energy and the thermal energy:

$$\Psi = \frac{\text{dipole–dipole contact energy}}{\text{thermal energy}} = \frac{\mu_0 \pi r_p^3 M^2}{9k_B T} \quad (12)$$

where  $k_B$  is the Boltzmann constant ( $1.3806 \times 10^{-23}$  J/K) and  $T$  (K) is the absolute temperature. Further insights into the physics of nanoparticle aggregation are discussed in Section 3.2.

Another effect favored by magnetophoresis is the hydrodynamic effect, wherein fluid flow is induced due to particle motion. Unlike cooperative magnetophoresis, which involves particle assembly, this effect occurs in cases where SPIONs are suspended in a solution at relatively low concentrations, resulting in insignificant interparticle magnetic dipole–dipole interactions [31]. Consequently, the magnetophoretic velocity of particles decreases to a low value. In this scenario, highly inhomogeneous magnetic field gradients are required to cause a concentration gradient of SPIONs within the fluid suspension. This concentration gradient subsequently induces convective flow in the fluid, leading to hydrodynamic effects driven by the interaction between the SPIONs and the fluid medium [32].

### 3. Magnetic Separation Process

#### 3.1. High-Gradient Magnetic Separation (HGMS)

Magnetic separation driven by magnetophoresis has been effectively implemented using the HGMS technique [33]. This technique commonly involves the utilization of packed columns of ferromagnetic (steel) material to capture the SPIONs. The packing materials in the columns typically possess diameters of approximately  $50 \mu\text{m}$  with gap distances ranging from  $10 \mu\text{m}$  to  $100 \mu\text{m}$  [34]. These materials exhibit a saturation magnetization of around 0.8 T and can establish high magnetic gradients on their surfaces, reaching values between  $10^4$  and  $10^5$  T/m when subjected to an external magnetic field [34]. During the operation of HGMS, once the column is magnetized by the external magnetic field, the SPIONs can be effectively trapped on the surface of the column, while the fluid carrying them can be collected at the outlet. This process can be repeated in cycles until the desired separation efficiency is achieved or until the column becomes saturated, indicating that no more particles can be deposited on the magnetic matrix. Subsequently, to recover the SPIONs, the external magnetic field is removed, causing the particles to be released from the column's surface. This enables the retrieval of the separated SPIONs for further utilization or analysis.

The high-gradient approach for magnetic separation offers several notable advantages: primarily, the technique's ability to generate exceptionally high magnetic gradients results in correspondingly elevated magnetic forces acting on the particles. This heightened magnetic force enables an increase in the flow rate, facilitating more efficient and rapid separation processes. Furthermore, HGMS has demonstrated its capability to successfully recover SPIONs with sizes as small as  $10 \text{ nm}$  [35]. This confirms the effectiveness of the technique in handling magnetic materials at the nanoscale level, making it particularly valuable for SPIONs separation and recovery applications. One of the most prominent

commercial implementations of HGMS is exemplified by the magnetic-activated cell sorting (MACS) systems devised by Miltenyi Biotec. This system employs a meticulously engineered setup wherein a substantial magnetic field gradient is established within a column tube [36]. The central component of this arrangement is a column densely packed with ferromagnetic stainless steel wool, suitably coated with a plastic material. Positioned within the field of a permanent magnet boasting an intensity of approximately 0.6 T, the steel wool column interfaces with the target cells [36]. In practice, cells previously labeled with superparamagnetic beads are introduced into the column. During the column's exposure to the magnetic field, magnetization ensues, rendering the steel wool fibers an exquisitely sensitive filter for magnetic particles, as presented in Figure 1. Consequently, the cells adhere to these steel wool fibers, achieving a magnetic-based separation. Subsequently, as the column is withdrawn from the external magnetic field, the magnetization of the particles dissipates, leading to the detachment of the particle-labeled cells from the steel wool. This, in turn, facilitates the elution of the solution, resulting in the attainment of a single-cell suspension. The MACS system epitomizes an advanced application of HGMS principles, adeptly harnessing magnetic forces for targeted cell sorting and manipulation.

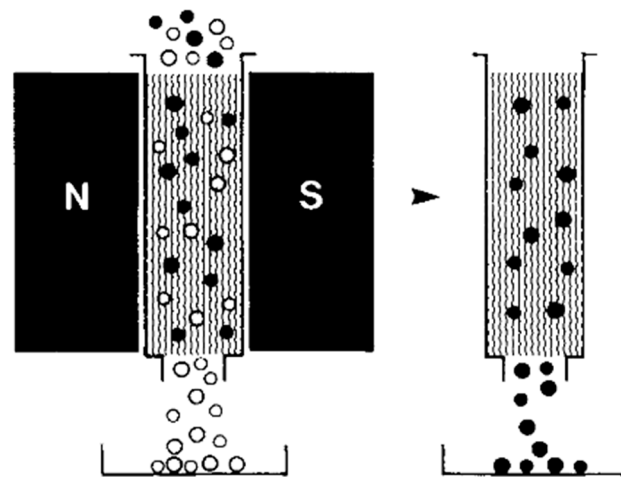


**Figure 1.** MACS by Miltenyi Biotec. The column containing steel wool is placed inside a magnetic field. Cells labeled with superparamagnetic beads are introduced to the system. Unlabeled cells are eluted, and the labeled cells can be collected by removing the external magnetic field. Reprinted with permission from [33], copyright 2005 John Wiley and Sons.

Despite the high capture efficiency of the HGMS approach, there exist certain drawbacks associated with its application. First, HGMS suffers from a range of practical limitations that involve installation and operational costs, which tend to be high, especially those related to power consumption on an industrial scale due to the need for electromagnets for generating the magnetic forces [34]. Second, the generation of inhomogeneous magnetic fields within the matrix presents a challenge in comprehending the intricate separation mechanism of SPIONs; the complexity of the column design further complicates the description and simulation of the SPION separation process, hindering comprehensive analysis when necessary. Another issue with HGMS lies in its lack of specificity in capturing particles, as some non-magnetic particles may inadvertently become trapped by the magnetic matrix, leading to an undesired contamination [37]. Moreover, certain SPIONs may experience permanent trapping within the system, making their recovery difficult or even unfeasible. These limitations need to be carefully addressed to enhance the overall effectiveness and practicality of HGMS in biomedical applications and other relevant fields.

### 3.2. Low-Gradient Magnetic Separation (LGMS)

In response to the limitations of HGMS, several research efforts in magnetic separation have focused on the development of LGMS. LGMS represents a cost-effective alternative capable of achieving separation using external magnetic field gradients typically on the

<100 T/m order. Additionally, a LGMS setup can be simpler to produce and operate compared to HGMS-based separators. This is because these fields and gradients can be created using just one permanent magnet or an arrangement of them, thus eliminating the need for magnetic packings inside the system. Due to its inherent simplicity and cost effectiveness, a substantial portion of current research is focused on understanding the fundamental principles that control the transport characteristics of magnetic nanoparticles under these low magnetic gradients [18,31,38].

In the presence of inhomogeneous magnetic fields generated by a permanent magnet, SPIONs move in the direction of the magnetic gradient, specifically to the region where  $\|\vec{B}\|$  is higher. In the case of a batch separation process, this migration results in the separation of SPIONs over a collection plane, allowing them to be extracted from the suspending medium, thereby concluding the separation process. However, this behavior is not limited to a particular type of magnetic field and applies to both inhomogeneous and homogeneous types of magnetic field gradients  $\vec{\nabla} B$ . The primary distinction between these two categories lies in the fact that  $\vec{\nabla} B$  remains constant in the latter case, while in both cases, there exists an inhomogeneous magnetic field. A quadrupole magnetic sorter (QMS) is a type of magnetic separator that generates a homogeneous magnetic field gradient, for example. One can notice that in the QMS, the intensity of  $\|\vec{B}\|$  changes in the radial direction as depicted in Figure 2, increasing toward the outer boundary of the central bore. In fact, the field generated by a QMS is expressed as follows [39]:

$$\|\vec{B}\| = \left(\frac{B_0}{r_0}\right)r \quad (13)$$

where  $B_0$  (T) and  $r_0$  (m) are the field magnitude at the bore or magnet's pole and the QMS radius, respectively, whereas  $r$  (m) represents the position or distance from the center of the bore. For the case of an inhomogeneous gradient, consider the one generated by a cylindrical permanent magnet of length  $L$  (m) and radius  $R$  (m). The magnetic field as a function of the axial distance  $x$  (m) along the horizontal axis can be approximated using the following expression [40]:

$$\|\vec{B}\| = \frac{B_r}{2} \left[ \frac{x+L}{\sqrt{(x+L)^2 + R^2}} - \frac{x}{\sqrt{x^2 + R^2}} \right] \quad (14)$$

where  $B_r$  (T) is the residual induction of the magnet. Figure 2 brings a comparison between the magnetic fields generated by a QMS and by a cylindrical permanent magnet according to the previous expressions.

The behavior of the magnetic field for both cases is distinct: while an inhomogeneous field gradient is generated by a field that decays rapidly in the horizontal direction, a homogeneous gradient generated by a QMS presents a field whose value linearly increases from the center to the wall of the separator. For the latter, it means that the field reaches its maximum value at the wall with a uniform and constant gradient throughout the radius of the bore. This type of magnet arrangement offers significant advantages in terms of simplifying the process characterization, modeling, optimization and scaling due to the straightforward estimation of the magnetic fields produced by the magnets positioned on the walls of the system. Furthermore, homogeneous gradients have been explored in the separation of magnetic nanoparticles and magnetically (labeled or unlabeled) biological materials in batch [30,35] and continuous flow [41–44] modes of operation. Batch magnetic separators collect particles on a collection plane or trapping element, which are subsequently retrieved through field removal; in contrast, continuous flow magnetic separators produce particle-concentrated streams by deflecting their trajectory based on differences between the magnetic susceptibilities of particles and the carrier fluid [18,44].

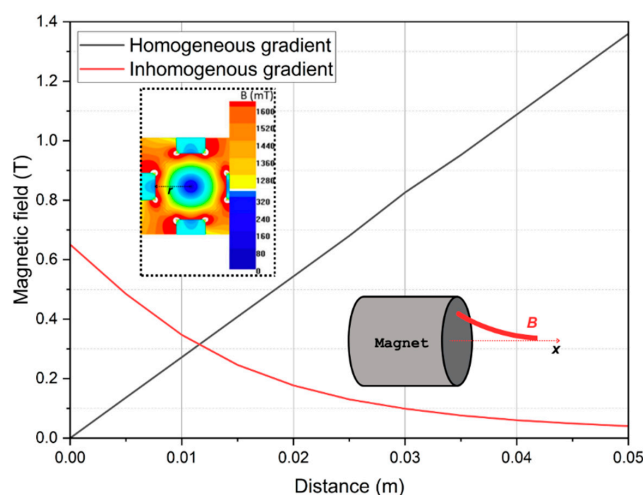


**Figure 2.** Comparison of illustrative magnetic fields generated by a QMS (black solid line) and a cylindrical permanent magnet (red solid line). For the QMS, a cross sectional magnetic field map (heat map of root mean square of  $B$ ) has been included in the plot for a device with  $B_0 = 1.68$  T and  $r_0 = 1.91$  mm, highlighting the high field that can be achieved inside these systems.

The study of the magnetophoresis of SPIONs in the context of LGMS has recently evolved to consider two distinct mechanisms that involve interparticle and particle–fluid interactions [45], as presented in Section 2. A frontier between these two types of interactions can be drawn essentially based on particle concentration levels. At relatively high concentrations, particle self-assembly (or reversible aggregation) is usually more expressive and can be predicted and analyzed through a series of parameters including the one expressed in Equation (12). This phenomenon is directly associated with higher magnetophoretic velocities of SPIONs aggregates since the magnetic force is size dependent, as indicated in Equation (8). Consequently, the increasingly augmented magnetic force acting on the aggregates can accelerate the separation process of SPIONs when exposed to low-gradient fields [12,30]. For this reason, the magnetic separation of SPIONs can be completed within a feasible time by employing a single or an arrangement of small permanent magnets. Conversely, at low concentrations, which is often the case for biological applications, the magnetic interactions may not be sufficient to induce particle aggregation and, in the case of LGMS, induced convection caused by particle motion may occur depending on the system’s dimensions and the magnitude of  $\nabla \vec{B}$  [31,40]. This phenomenon has been observed through simple dye-tracing experiments and evaluated parametrically via numerical simulations of fluid dynamics [31,45].

The observation of relatively short separation times by researchers that have explored low-gradient conditions to magnetically separate SPIONs (<50 nm) [29,30,35,46,47] contrasts with the classical approach of magnetophoresis that assumes non-interacting particles. In these studies, separation times of minutes or hours were observed by applying gradients as low as 13 T/m [48]. The classical approach to magnetophoresis, which assumes non-interacting particles, can be fair for high-gradient conditions; however, it is unsuitable for low-gradient applications [49]. For the majority of LGMS applications, the magnetophoretic velocity estimated through the classical approach is too low to be considered viable for separation, which would lead to practically unachievable separation times even for small volumes [31,49]. More elaborate physical models must be considered to properly describe particle magnetic interactions that lead to observations related to the concentration dependence of magnetophoresis [49,50] caused by the aggregation of magnetic nanoparticles.

To gain a more profound comprehension of the fundamental physical aspects involved in particle aggregation or self-assembly phenomenon, one may consider starting from the

magnetic force exerted upon a single, superparamagnetic nanoparticle, which is saturated at its saturation magnetization value ( $M_p$ , A/m) by a magnetic field gradient  $\nabla H$  (A/m) [29]:

$$F_{\text{mag}} = \mu_0 V_p (M_p \cdot \nabla) H \quad (15)$$

where  $V_p$  ( $\text{m}^3$ ) is the particle volume. Upon magnetized, the magnetic nanoparticles start to generate a surrounding magnetic field, similar to the idea of “nanomagnets”, which will interact with other surrounding magnetic fields, ultimately causing attracting magnetic forces that, under specific conditions, may result in particle aggregation in larger clusters or chains, or even agglomerates thereof [51]. Considering the case of agglomerates with a spherical shape, Equation (15) scales up via the aggregation parameter ( $N^*$ ) through:

$$V_c = V_p N^* (\varphi_0, d_p) = \frac{4}{3} \pi r_p^3 \cdot N^* (c_p^m / \rho_p, d_p) \quad (16)$$

where  $V_c$  ( $\text{m}^3$ ) is the cluster/agglomerate volume,  $d_p$  (m) is the particle diameter,  $c_p^m$  (g/L) is the mass concentration of particles,  $\rho_p$  is the particle density ( $\text{kg}/\text{m}^3$ ), and  $\varphi_0$  refers to the volume fraction of particles (equal to  $c_p^m / \rho_p$ ). Notably, during self-assembly, the cluster volume  $V_c$  becomes larger and, according to Equation (15), the resulting magnetic force is expected to exhibit a proportional relationship with  $V_c$ , thus causing larger magnetophoretic velocities on these agglomerates. The aggregation parameter  $N^*$  is a dimensionless group commonly employed as an indicative of the occurrence of particle aggregation [51,52]:

$$N^* = \sqrt{\varphi_0 e^{(\Psi-1)}} \quad (17)$$

The term  $\Psi$  in Equation (17) represents the ratio between the magnetic dipole–dipole and thermal energies and is calculated using Equation (12). The dipole–dipole energy on the numerator depends directly on the particle size (in this case,  $r_p$ ) and the saturation magnetization constant  $M_p$ , while the randomizing thermal energy term  $k_B T$  is essentially associated with Brownian motion [53]. For particle aggregation to occur, the former must surpass the latter to ensure that the separation system can benefit from particle aggregation. Following, the threshold for self-assembly of magnetic nanoparticles is  $N^* = 1$ , for when  $N^* < 1$ , the generation of clustered structures either in spherical or chain form is mitigated by the system’s entropy; in contrast, when  $N^* > 1$ , particles are increasingly more likely to reorganize into various agglomerates [45]. An alternative way to predict the field-induced self-assembly of magnetic nanoparticles in a LGMS system (or HGMS) is to compare the average distance between particles  $d_{p,p}$  (m) and the magnetic Bjerrun length  $\lambda_B$  (m), mathematically written as follows:

$$d_{p,p} = 2.7 \frac{d_p}{6\varphi_0^{1/3}} \quad (18)$$

and

$$\lambda_B = d_p \cdot \Psi^{1/3} \quad (19)$$

The length scale  $\lambda_B$  denotes the distance required for  $\Psi$  to attain a value of 1 in Equation (12), thus indicating a balance between dipole–dipole interaction energy and thermal energy [35]. The existing literature establishes a comparative framework for these parameters, wherein particle aggregation is facilitated when  $\lambda_B \gg d_{p,p}$  or the product  $\varphi_0 \Psi \gg 0.1$ . Conversely, if  $\lambda_B \ll d_{p,p}$  or the term  $\varphi_0 \Psi \ll 0.1$ , then entropy is dominant and the system is dominated by a random diffusion mechanism, which is detrimental to a successful magnetic separation. In the context of magnetic separations, rather small particle sizes are associated with difficult separations to accomplish; in the case of SPIONs, this limit is in the vicinity of 40 nm [54]. At this scale, the influence of random thermal energy becomes predominant, impeding the magnetically guided motion of particles.

Consequently, achieving rapid magnetic separation necessitates the occurrence of particle aggregation or self-assembly.

Using an external magnetic field gradient for particle manipulation purposes has significant appeal in various engineering applications, especially in environmental remediation and water treatment, as well as in biomedicine [55]. The current success of LGMS for biological applications is the result of advancements in synthesizing colloidal stable nanoparticles and various surface functionalization techniques that enable the selective adsorption of specific target entities [45,56]. For instance, target entities in bioseparation applications are cells or pathogens, such as viruses and bacteria, which are inherently diamagnetic (nonmagnetic), and, therefore, it is crucial to magnetically label these entities with magnetic nanoparticles modified with specific functional groups to enable attachment [57]. Selective targeting and separation of bio-agents or molecules using LGMS techniques can find applications in disease diagnosis, for example, that of cancer [58–60] and infection via the separation of bacteria [61]. Furthermore, particle self-assembly can be beneficial to certain biomedical applications, such as the design of fast diagnostic methods based on cell labeling. In this sense, the cooperative behavior of SPIONs during a LGMS process may be the basis for an alternative way to reduce the separation time of magnetically labeled target entities [62]. In this context, from Equation (18), it is fair to consider that, as the particle concentration in a dispersion increases, the average distance between suspended nanoparticles decreases. This reduction in interparticle distance causes an augment in magnetic dipole–dipole interactions, leading to potential particle aggregation when highly concentrated SPION solutions are used. Indeed, it has been recently shown that, through batch separation experiments of 20 nm and 30 nm SPIONs at various initial concentration values of the particle dispersion, higher initial concentrations of SPIONs enhanced the magnetophoretic separation time [63]. However, for an optimal operation of this principle, one must consider the economic viability of the process, since highly concentrated solutions can be detrimental to the process economy and become environmentally non-friendly.

Even though the reversible aggregation of magnetic nanoparticles plays an important role in increasing their magnetophoretic velocity when exposed to a low magnetic gradient, effectively separating SPIONs using LGMS techniques is still a considerable challenge due to the relatively low magnetic field gradient and, as a result, the low magnetic force [49]. Furthermore, overcoming physical barriers of LGMS in the form of Stokes drag and Brownian motion still represents a challenge as particle size has decreased in the last few decades in many applications as a response to an optimization process and a crescent demand of small particle sizes in various sorts of applications [49,64]. These limitations can often require extended magnetic exposition periods for separation in LGMS systems, ranging from several hours to days depending mostly on particle size and concentration [29,30,62]. Despite these challenges, LGMS holds promise as a cost-effective alternative in magnetic separation research for specific applications.

## 4. Applications of SPIONs

### 4.1. Drug Delivery

One of the most prominent and sought-after applications of SPIONs is their role in targeted drug delivery, particularly in the realm of cancer treatment [65]. The utilization of SPIONs in drug delivery was first documented in the scientific literature in 1960 when Freeman et al. posited the hypothesis that SPIONs could be conveyed through the vasculature and selectively accumulated in a designated anatomical region through the application of a magnetic field [66]. In the 1970s, Senyei et al. engineered albumin microspheres incorporating SPIONs, demonstrating their ability to be effectively retained under in vivo capillary flow conditions using a magnetic field [67,68]. Additionally, innovative drug delivery systems have been devised utilizing drug-coated magnetic beads. Lubbe et al. achieved successful deployment of a ferrofluid containing drugs in an in vivo mouse model, demonstrating its efficacy as an anti-tumor agent with an absence of observed toxic effects [69]. In this drug delivery paradigm, SPION surfaces are deliberately

functionalized with specific groups, such as polymethyl methacrylate (PMMA) or polyethylene glycol (PEG), subsequently enabling the loading of therapeutic drugs [70]. Recent advancements in SPION-assisted drug delivery systems have particularly emphasized the transportation of peptides, chemotherapeutic agents, and radioactive drugs [71]. In these intricate systems, surface-engineered SPIONs, alongside the encapsulated drugs, are directed to the designated target site through the influence of an external magnetic field. Subsequently, a controlled release of the drug occurs at the local site of interest. A notable advantage of this approach lies in its potential to reduce the necessary drug dosage and minimize adverse side effects [72]. For these applications, factors such as size, surface chemistry, and the toxicity of the SPIONs are of paramount significance. These characteristics must be carefully considered to ensure the prolonged circulation of the SPIONs within cellular environments. It is crucial to acknowledge that as the SPIONs reside within cells, the coating could undergo digestion, potentially affecting the overall cellular integrity [73]. Therefore, meticulous attention to these properties is imperative to facilitate successful and safe SPION-based drug delivery systems. Figure 3 illustrates the sequential process involved in utilizing SPIONs for drug delivery in the context of cancer treatment. This methodology typically comprises a two-step procedure: initially, the SPIONs undergo functionalization through the attachment of diverse ligands, including drug carriers. Subsequently, these modified SPIONs are capable of binding with the specific drug molecules of interest. Finally, the engineered SPIONs are released into the biological milieu, moving toward the intended target cells. Once these have reached their destination, the SPIONs achieve a controlled release of their anticancer agents, thereby contributing to the therapeutic objective of tumor destruction [74].

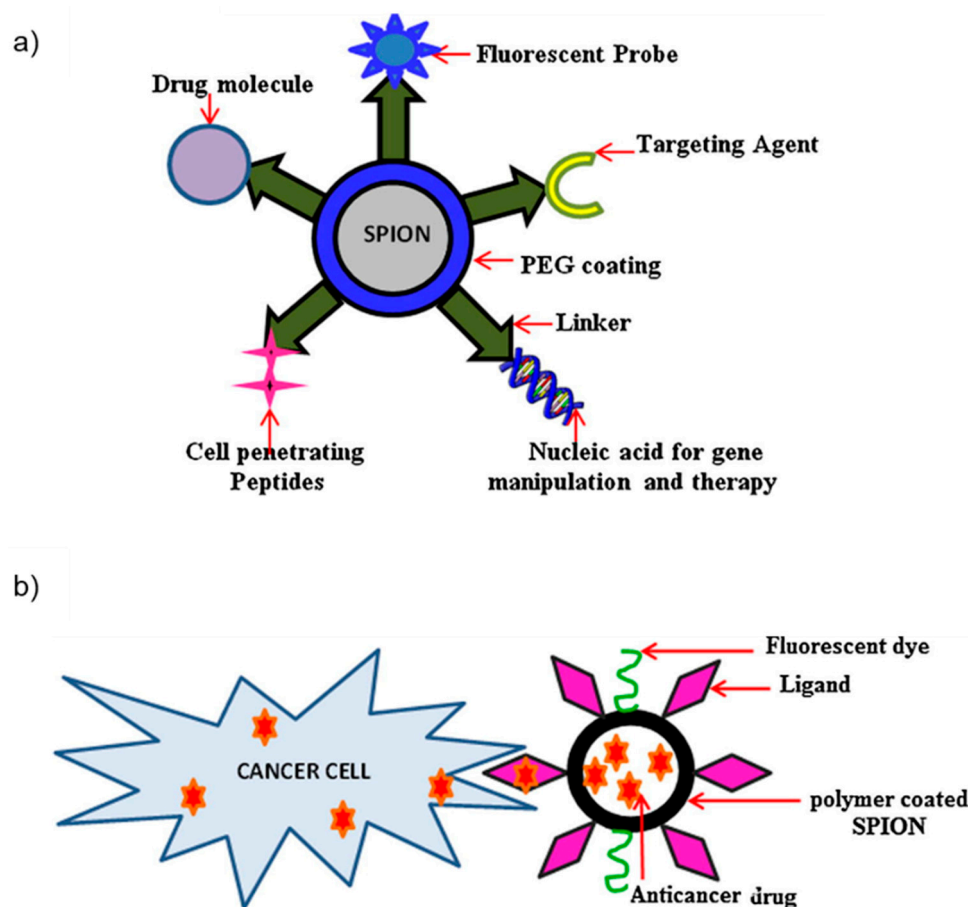


**Figure 3.** Representative schematic process of SPION utilization in drug delivery for cancer treatment. (a) SPIONs functionalized with multiple ligands. (b) Tumor targeting using engineered SPIONs. Reprinted with permission from [63], copyright 2013 Elsevier.

One common use for SPIONs in drug delivery is for cancer treatment [60]. In the investigation conducted by Ayubi et al., the focus was on the examination of hydrophobic anticancer pharmaceutical compounds [75]. In their research, the authors employed SPIONs characterized by surface modification through the introduction of PEGylated curcumin (PEG-Cur). Curcumin (Cur), as an integral component of this endeavor, was subjected to conjugation via N-ethyl-N'-(3-(dimethylamino)propyl)carbodiimide/N-hydroxysuccinimide (EDC/NHS) chemistry to the PEG functional groups, thereby being physically tethered to the nanoparticles' surface. The synthesized SPIONs exhibited a mean diameter within the range of 24.33 to 34.24 nm. Furthermore, the saturation magnetization of these nanocomposites was measured to be 59 emu/g, a magnitude significant enough to facilitate a responsive reaction to external magnetic fields. Furthermore, the authors asserted the absence of coercivity in the hysteresis loops, demonstrating the superparamagnetic nature of the SPIONs. Remarkably, Ayubi et al. showed that these SPIONs demonstrated the highest attainable drug release percentages under both neutral (43.7%) and acidic (53.5%) media conditions. In addition to the foregoing findings, they conducted assessments to validate the biocompatibility of the nanomaterials. These assessments included LD50 (lethal dose 50%) analysis and hemolysis analysis, collectively affirming the favorable biocompatibility profile of the SPIONs. This exemplifies the proficient application of SPIONs in drug delivery, showcasing elevated efficacy and compatibility with biological systems through the controlled modulation of an external magnetic field. Another example is the study carried out by Kumar et al., where iron oxide nanoparticles coated with citric acid were synthesized and subsequently dispersed in an aqueous medium [76]. The anticancer drug doxorubicin (Dox) was non-covalently linked to these citric acid-coated SPIONs. The synthesized SPIONs exhibited an average diameter of approximately 12 nm. The investigation revealed a sustained release profile of the conjugated Dox from the nanoparticles. The cellular internalization of Dox-coated SPIONs was facilitated through the application of a magnetic field using a bar magnet. Employing an external magnetic field as a guiding force enabled the successful incorporation of Dox-coated SPIONs into cellular entities. Furthermore, the cellular uptake of these SPIONs was observed to be substantial, indicating their potential for therapeutic applications in cancer treatment. Moreover, in the study conducted by Perillo et al., multifunctional MNPs were meticulously engineered, featuring a core composed of SPIONs with multiple stratified coatings, and subsequently functionalized with the desired cell-penetrating peptide (CPP) [77]. The resulting CPP-capped MNPs exhibited an average diameter of 98 nm and a zeta potential of 4.08 mV. Due to their sizes (smaller than 100 nm), the SPIONs could successfully reach tumor sites where they accumulated with the assistance of a magnetic field. Through comprehensive in vitro assessments, the authors elucidated that the predominant cellular uptake mechanism for these particles was endocytosis. This discerned mechanism holds significant implications for the potential applications of these functionalized SPIONs in the realm of cancer theragnosis, representing a promising avenue for further research and clinical translation.

In addition to cancer treatment, SPIONs can also be applied for the load and subsequent release of drugs for antibacterial therapeutics. One example is a recent study conducted by Zhang et al., who introduced an innovative antibiotic delivery system, wherein they utilized silica-coated SPIONs that were covalently linked to a CPP through a co-deposition method [78]. Subsequently, a polyvinyl alcohol (PVA) polymer coating was applied via physicochemical binding. The antibiotic of interest, vancomycin (VAN), was effectively loaded onto these synthesized particles. The investigation revealed a progressive reduction in the magnetic properties of the composite entity as successive layers of supplementary coatings were added to the nanoparticle core. Despite the diminishing magnetic attributes, the coated SPIONs maintained their superparamagnetism, with a saturation magnetization of 40 emu/g. The particles were recovered from concentrated solutions of VAN via the utilization of an external magnet. The investigators asserted that these engineered MNPs exhibited the capability to undergo internalization into both *Escherichia*

*coli* (*E. coli*) and *Staphylococcus aureus* (*S. aureus*) bacterial cells. Moreover, this unique conjugation of SPIONs with VAN was shown to significantly enhance the antimicrobial activity of the drug. This promising antibiotic delivery system represents a potential advancement in the field of antibacterial therapeutics.

Table 1 presents some studies in which SPIONs have been used in drug delivery in the past six years.

**Table 1.** An overview of recent studies using SPIONs for drug delivery.

Particle Composition Size (nm)	Particle Properties	Drug	Drug Loading Method	Specificities	Ref.
Iron oxide 12	Coated with citric acid	Anticancer drug Dox	Noncovalent interaction	Cellular internalization of Dox-coated SPIONs was facilitated using a bar magnet.	[76]
Fe <sub>3</sub> O <sub>4</sub> 500	Functionalized with PEG-COOH; M = 23.54 emu/g	Insulin	Covalent bond	Magnetic separation of SPIONs happened within 30 s under external magnetic fields.	[79]
Iron oxide 24.33–34.24	Coated with PEG-Cur; M = 59 emu/g	Cur	-	SPIONs were biocompatible and had the highest attainable drug release percentages under both neutral (43.7%) and acidic (53.5%) media conditions.	[75]
Fe <sub>3</sub> O <sub>4</sub> 105.7 ± 3.81	Conjugated with BSA <sup>1</sup> ; Zeta potential = -18.2 mV	MTX <sup>2</sup>	-	MTX release from Fe <sub>3</sub> O <sub>4</sub> @BSA-MTX showed an enzyme-dependent release pattern.	[80]
Fe <sub>3</sub> O <sub>4</sub> 56 ± 11.43	Coated with BSA; Zeta potential = -10.1 mV	Cur	Desolvation and chemical co-precipitation	Particles were biocompatible and demonstrated an inhibitory effect on cancer cells in 72 h.	[81]
Fe <sub>3</sub> O <sub>4</sub> 32	Coated with silica and PVA; Conjugated with CPP	VAN	-	An external magnet was used to recover the particles from a concentrated solution of VAN.	[78]
Iron oxide 87.17 ± 1.14	Labeled with Cy5.5 <sup>3</sup> ; Coated with PEG; Zeta potential = -5.68 mV	gH625-derived peptide	Covalent thio-ether bonds	SPIONs could successfully reach tumor sites and accumulate there with the application of a magnetic field.	[77]
Fe <sub>3</sub> O <sub>4</sub> 5–15	Coated with PVA	Sorafenib	-	SPIONs were superparamagnetic and the cellular uptake studies suggested their efficient entrapment in HepG2 cells.	[82]

<sup>1</sup> Bovine Serum Albumin; <sup>2</sup> Methotrexate; <sup>3</sup> Cyanine 5.5.

#### 4.2. Cell Separation and Sorting

Magnetic cell separation has gained significant attention as a prominent technique for the isolation of specific cells, particularly those of rare occurrence, from heterogeneous cell populations [83]. This method revolves around the utilization of SPIONs that are conjugated with precise antibodies capable of binding to target cells. Notably, the application of magnetic cell separation has been most extensively employed in the isolation of stem cells [84] and cancer cells [85]. The utilization of magnetic separation for the isolation of biological entities was initially employed in the 1970s for cell sorting [83]. Since then, magnetophoresis has become a pervasive technique for the targeted separation of specific cells from a given biofluid [86]. This approach capitalizes on the distinctive attributes of SPIONs, allowing for the segregation of magnetically labeled cells when subjected to an external magnetic field [87]. Consequently, the inherent magnetic property of SPIONs significantly influences the magnetophoretic mobility of magnetically labeled cells, rendering it a pivotal parameter distinguishing these labeled cells from their unlabeled counterparts. By harnessing this unique magnetic behavior, magnetic cell separation offers a powerful and precise methodology for the selective isolation of specific cell subpopulations. Figure 4 represents a general process of magnetic cell separation using SPIONs, including three steps: magnetic labeling, magnetic trapping, and the release of target cells.

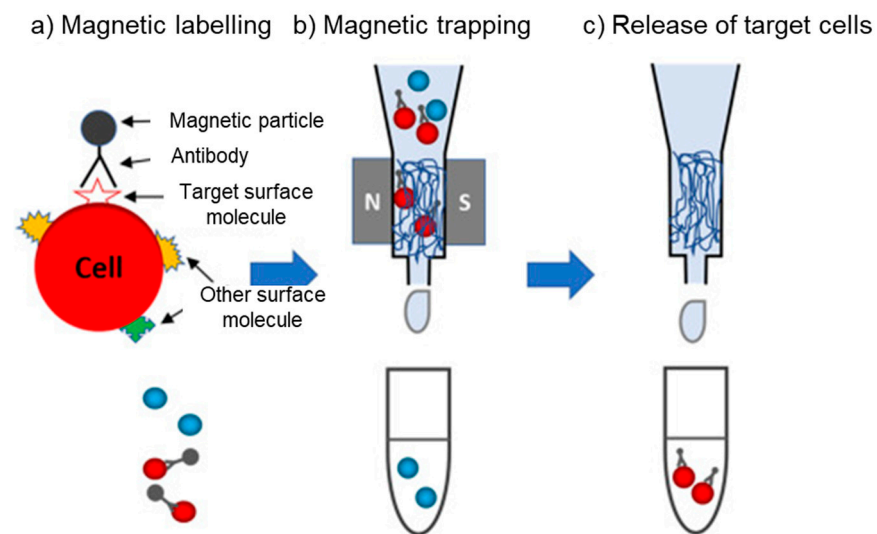


**Figure 4.** Schematic process of magnetic cell separation using SPIONs. (a) Magnetic labeling of target cells with SPIONs as well as specific biomarkers. (b) Separation of target cells using a magnetic field. (c) Release of target cells after removal of the magnetic field. Reprinted with permission from [76], copyright 2022 Elsevier.

The application of SPIONs for magnetic cell separation has gained more attention for the isolation/separation of tumor cells. For instance, in the study conducted by Zhou et al., SPIONs were employed to isolate circulating tumor cells (CTCs) (as shown in Figure 5a) [88]. Within their experimental setup, the anti-epithelial cell adhesion molecule (anti-EpCAM) antibody was introduced into the system through the use of a linker containing disulfide bonds. Quantum dots (QDs) were subsequently deposited onto  $\text{Fe}_3\text{O}_4$  nanoparticles. These MNPs exhibited a uniform size distribution with an average diameter of  $301.2 \pm 29.9$  nm and a notably high saturation magnetization of  $64.53$  emu/g. Upon the application of a magnetic field, the CTCs were successfully isolated from blood samples, achieving capture efficiencies exceeding 90%. This efficient isolation process was achieved within a remarkably short timeframe, with the isolation of CTCs ranging from 5 to 200 CTCs per mL taking only 1–2 min. Importantly, the SPIONs utilized in this study were found to be recoverable through magnetic means. The authors contended that these functionalized SPIONs represent a potent platform for CTC isolation, offering substantial promise for applications in cancer research and diagnostics.

Another example is the study conducted by Payer et al., where the authors devised a novel technique for gentle flow separation employing carboxymethyl-dextran (CMD)-coated SPIONs in conjunction with a LGMS system [89]. The SPIONs employed in this work were synthesized from  $\text{Fe}_3\text{O}_4$  using a wet chemical precipitation technique, exhibiting a core diameter of 25 nm. Additionally, the SPIONs possessed a saturation magnetization of 73 emu/g, a magnitude deemed adequate for separation via LGMS. Subsequent to the incubation of breast cancer tumor cells with these SPIONs, a permanent magnet was employed to effectuate magnetic separation. The magnetic separation procedure was performed by employing a magnet in conjunction with a blood bag. Subsequent to introducing the labeled cell suspension into the blood bag, the negative fraction was eluted from the separator, while the positive fraction (labeled cells) was retained within the separator. The latter was later collected through the removal of the magnet. The researchers reported remarkable outcomes, asserting an exceptional depletion efficiency of tumor cells. Specifically, their results demonstrated a reduction to less than 3% of tumor cells remaining in 24 h stored blood samples and an even more modest proportion, equal to or less than 14%, in freshly obtained blood samples. These findings underscore the potential of their approach for an efficient isolation and removal of tumor cells from biological specimens.

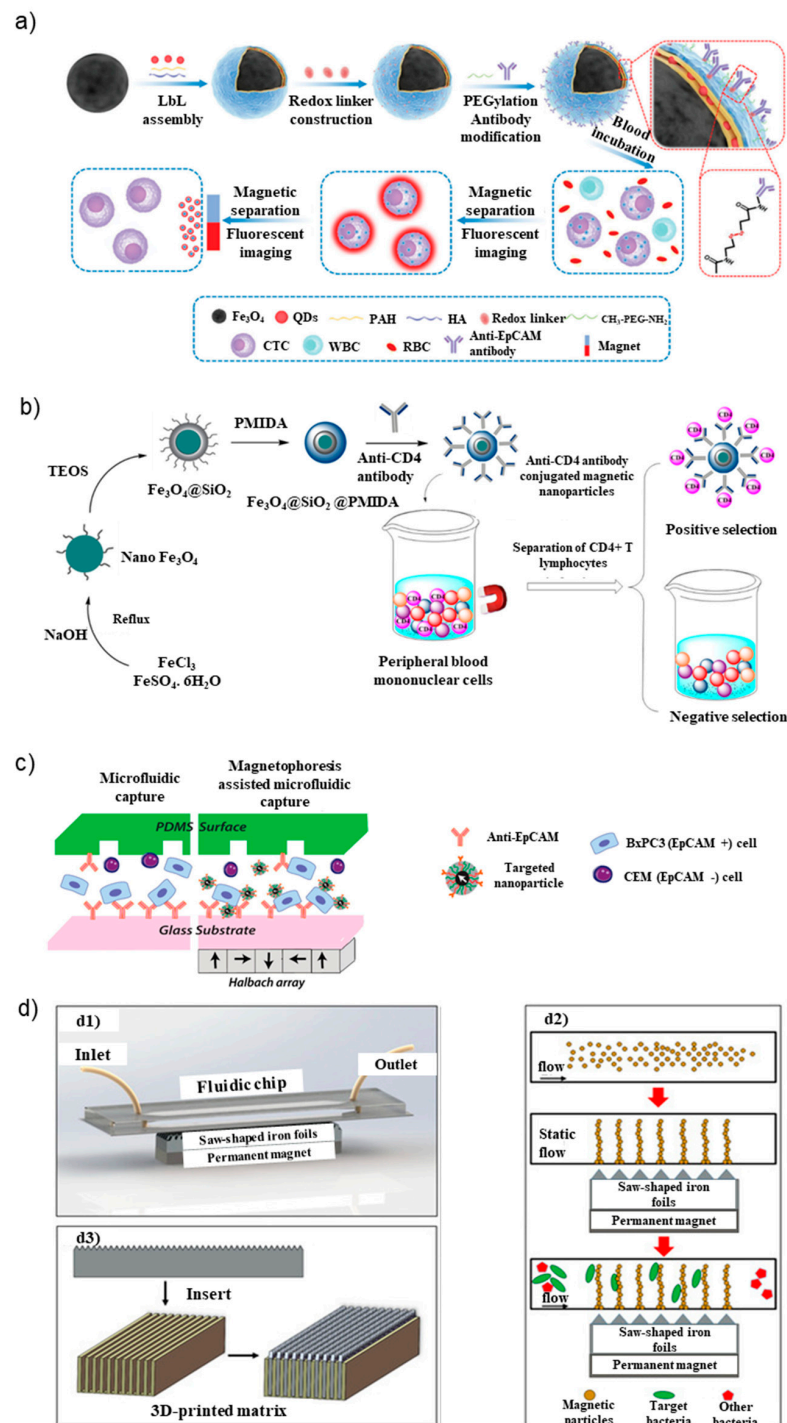


**Figure 5.** Representation of recent research on SPIONs application for cell separation: (a) Preparation process of PEGylated immunomagnetic nanospheres and the CTC separation process from blood using these particles. Reprinted with permission from [77], copyright 2012 Royal Society of Chemistry. (b) Schematic process of using  $\text{Fe}_3\text{O}_4@SiO_2$  to separate CD4+ T lymphocytes. Reprinted with permission from [81], copyright 2020 Elsevier. (c) Schematic of a tumor cell separation process using the combination of SPIONs and a magnetophoresis-assisted microfluidic array. Reprinted with permission from [80], copyright 2020 Elsevier. (d) Schematic view of the device employed for magnetic separation of target bacteria using SPION chains (d1), showing the formation of chains and the separation of target bacteria (d2), and the configuration of the iron foils (d3). Adapted with permission from [82], licensed under a Creative Commons Attribution 4.0 International License.

Moreover, in the study conducted by Saei et al., an innovative and notably efficient methodology was devised for the isolation of tumor cells from freshly obtained whole blood [90]. This approach leveraged the utilization of SPIONs synthesized via a specific protocol. The SPIONs were produced through the coprecipitation method. In this process, iron oxide core nanoparticles were synthesized and subsequently coated with citrate. This coating served the dual purpose of preventing self-aggregation and offering potential attachment sites for ligands. These SPIONs were subsequently functionalized with antibodies specifically targeting the Human Epithelial Growth Factor Receptor 2 (HER2). The authors postulated that these antibody-conjugated MNPs possessed a remarkable affinity for HER2-positive cancer cells, rendering them capable of selectively binding to such cells in a highly exclusive manner. This unique feature of the antibody-conjugated SPIONs positioned them as exceptionally efficient agents for the isolation of individual cancer cells, representing a significant advancement in the field of single-cell separation techniques. Moreover, the superparamagnetic characteristics of these SPIONs render them a promising candidate for expeditious target cell separation.

In the study conducted by Unni et al., SPIONs composed of iron oxide, surface-modified with PEG, and conjugated with antibodies against EpCAM through the avidin-biotin chemistry approach were employed for cancer cell separation [91]. The SPIONs employed in this study were synthesized through the semi-batch decomposition method using iron oleate as the precursor, yielding particles with a magnetic diameter of  $18.1 \pm 0.7$  nm. The research team's primary objective was to evaluate the specificity of these engineered MNPs for cancer cell separation, focusing on EpCAM-expressing tumor cells, notably the BxPC3 cell line. The magnetic separation procedure of the labeled cells was executed by employing a microfluidic device with the magnetic field gradients produced via a planar Halbach array. The Halbach array, characterized by a distinctive configuration of permanent magnets, served to enhance the magnetic field gradients generated in specific regions of the device. Experimental findings demonstrated that the designed SPIONs exhibited a high degree of specificity in their interaction with EpCAM-expressing tumor cells, specifically BxPC3 cells. Furthermore, the utilization of Halbach magnetostatic arrays proved effective in the separation of BxPC3 cells labeled with the engineered MNPs, as shown in Figure 5c.

Besides the utilization of SPIONs in tumor cell separation processes, some researchers have conducted important studies on the isolation of other cell populations. For example, Rashid et al. have introduced a novel MACS platform for the isolation of peripheral blood T CD4+ lymphocytes [92]. The platform leverages the utilization of  $\text{Fe}_3\text{O}_4$  MNPs encapsulated within a  $\text{SiO}_2$  shell, surface-functionalized with N-(phosphonomethyl) iminodiacetic acid (PMIDA), and subsequently conjugated with anti-CD4 monoclonal antibodies. The  $\text{Fe}_3\text{O}_4$  MNPs were prepared via the co-precipitation method. The functionalized SPIONs exhibited an average size of approximately 60 nm. The engineered SPIONs exhibited superparamagnetic characteristics via an inspection of their hysteresis loops. Owing to their superparamagnetism and substantial saturation magnetization value, these nanoparticles could be readily separated from the solution using an external magnetic field. Remarkably, the authors reported the successful isolation of T CD4+ lymphocytes from whole blood samples using a permanent magnet. This isolation process achieved notably high levels of purity, underscoring the efficacy of this MACS-based methodology for the specific isolation of T CD4+ lymphocytes from complex biological samples, as shown in Figure 5b.

Finally, in the research conducted by Cai et al., an investigation was undertaken to explore the separation of *Salmonella syphimurium* (*S. syphimurium*) utilizing self-assembled SPIONs possessing a diameter of 150 nm [93]. These MNPs were carboxyl modified and functionalized with polyclonal antibodies specifically designed to target the pathogen. To facilitate the separation process, a permanent magnet was employed as the driving force, as shown in Figure 5d. Concretely, a magnetic field separator employing a dot array, characterized by laminated sawtooth-shaped iron foils and a permanent magnet, was employed for the generation of the SPION chains. Remarkably, the results of this experimental approach

demonstrated an impressive separation efficiency, with approximately 80% of the target bacteria being successfully isolated within a relatively short duration of 45 min.

Table 2 provides recent studies published within the last seven years in which SPIONs have been used for the selective isolation of cells.

**Table 2.** An overview of recent studies using SPIONs for cell separation.

Particle Composition Size (nm)	Particle Properties	Magnetic Field Source	Target Cell Type	Efficiency	Ref.
Fe <sub>3</sub> O <sub>4</sub> 301.2 ± 29.9	Modified with fluorescent QDs; Conjugated with anti-EpCAM antibodies	Permanent magnet	MCF-7 cells and HepG2 cells	90%	[88]
Fe <sub>3</sub> O <sub>4</sub> 25	Coated with CMD; M = 73 emu/g	Permanent magnet	Circulating epithelial tumor cells	97%	[89]
Fe <sub>3</sub> O <sub>4</sub> 30	Coated with SiO <sub>2</sub> shells; Modified with PMIDA	Permanent magnet	T CD4+ lymphocytes	93.30%	[92]
Fe <sub>3</sub> O <sub>4</sub> 84.9	Conjugated with anti-HER2 antibodies; Zeta potential = −36.5 mV in pH = 7.4 Coated with PEG;	NdFeB magnet	BT474, BT474/MCF7	94.5 ± 0.8% 70.6 ± 0.4%	[90]
Iron oxide 20.3 ± 1.5	Modified with streptavidin-biotinylated anti-EpCAM antibodies	Halbach array (N52 magnets)	BxPC3 cells	75%	[91]
Iron oxide 12–47	Conjugated with anti-CD20 antibodies; Zeta potential = −10 mV at pH = 11	Permanent magnet	CD20-expressing lymphoma cells	95%	[94]
Iron oxide 150	Modified with carboxyl groups	NdFeB N42 magnets 0.2 T, 300 T/m	<i>S. typhimurium</i>	80%	[93]
Fe <sub>3</sub> O <sub>4</sub> 200	Polydopamine-coated porous MNPs	NdFeB magnet	Methicillin-resistant <i>S. aureus</i>	99%	[95]

#### 4.3. Environmental Remediation

Nanotechnology and nanoparticles have emerged as pivotal contributors to the field of environmental remediation, particularly within the context of water and wastewater treatment [96]. The growing occurrence of various contaminants, including heavy metals, organic substances, and radioactive elements in water systems due to industrialization and population growth, emphasizes the pressing need for efficient methods to address and resolve this issue. Figure 6 illustrates the diversity of types of nanoparticles that have shown to be capable of being used for water remediation, specifically via adsorption [97]. In this context, SPIONs have garnered significant recognition, particularly in the context of mitigating diverse organic contaminants such as dyes and pesticides, as well as heavy metals, pathogenic microorganisms, pharmaceuticals, and nano-/microplastics [98,99]. An inherent advantage of employing SPIONs in wastewater treatment is attributed to their iron-based composition that confers not only magnetic properties but also heightened reactivity toward pollutant removal. Indeed, iron can act as a potent reducing agent, facilitating the breakdown of various organic or inorganic pollutants into less harmful substances [100]. Moreover, the extensive surface areas of these nanoparticles, combined with their reactive and catalytic properties, have prompted various research studies on their use as standalone materials in water treatment or incorporated into mixed matrix nanocomposites.

The surging appeal of nanoparticles for environmental remediation can be attributed to their surface-driven mechanisms and their ability to be customized for specific applications through different coatings. Non-coated SPIONs exhibit hydrophobic characteristics, chemical instability, aggregation, and limited biodegradability, being therefore mostly unsuitable for water remediation purposes [101]. Through an appropriate incorporation of coatings, SPIONs can be functionalized and become nano-adsorbents, which can selectively remove a wide range of pollutants [10]. The separation process involving the temporary binding of a target component to the magnetic nanoparticle surface is known as sorption [101–103], which comprises several steps [97,104,105]. Upon the binding of the contaminants to the functionalized surface/pores of SPIONs, these magnetic nanoparticles can either form reversible bonds with the target species (general adsorption processes) or promote their destruction via advanced oxidation processes (AOPs). Thus, the contaminants can be either efficiently extracted from the liquid medium through the application of external magnetic field gradients to induce the magnetophoretic separation of SPIONs that adsorbed a specific target on their surface or destroyed via the promotion of AOPs by the particles. Subsequently to the general adsorption process (no AOPs), through a

process of desorption, contaminants can be effectively released from SPIONs, allowing for the restoration of their separation capability for successive treatment cycles [106]. In the case of AOPs, the particles do not need to undergo desorption as the contaminants become degraded during the process, as depicted by Figure 7, which refers to the photocatalytic degradation of pollutants caused by magnetic nanophotocatalysts (MNPCs) [19,107,108].

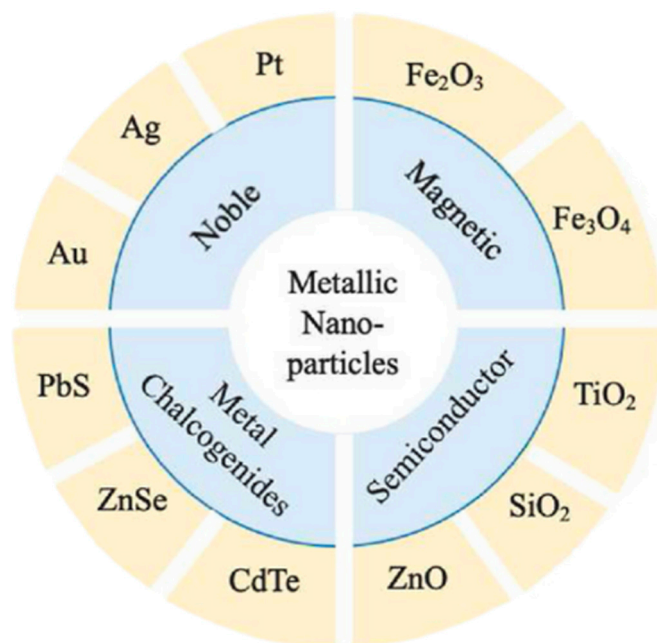


**Figure 6.** Classification of different metallic nanoparticles with adsorbent capabilities. Adapted with permission from [97], copyright 2022 Elsevier.

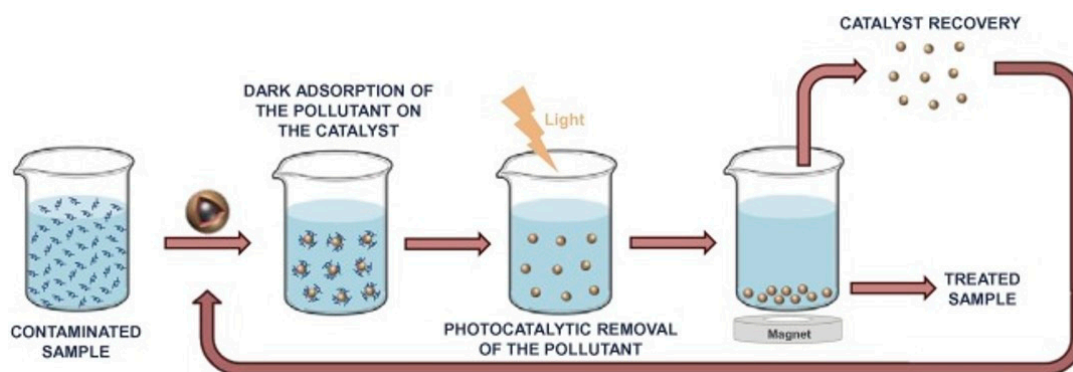


**Figure 7.** Photocatalytic removal of pollutants using MNPCs: the same material can be used for multiple cycles, maintaining nearly the same efficacy in degrading pollutants. However, after a certain number of recycling stages, the MNPC typically exhibits a slight reduction in its activity. Reprinted with permission from [16], copyright 2017 Elsevier.

The use of MNPCs in water treatment has recently been the focus of significant interest due to the improved physical and chemical characteristics of these substances. MNPCs are a type of advanced material that can be used to remove dyes and organic compounds from water through photocatalytic mechanisms [100]. The photocatalytic process works by using light to trigger the electronic reconfiguration of the material involved. Briefly, when a photon possessing an energy equal to or greater than the band gap energy is absorbed, it excites electrons from the valence band to the conduction band in the material, simultaneously creating a photogenerated hole [19]. This results in the promotion of a series of reactions that produce reactive oxygen species such as superoxide anions ( $O_2^-$ ) and hydroxyl radicals ( $\bullet OH$ ) on the surface of the material, which can oxidize organic pollu-

tants [108]. The semiconductors that have been predominantly utilized as photocatalysts are TiO<sub>2</sub> and ZnO [100]. However, other materials have proven relevant in the field [109]. Moreover, SPIONs have been used for the degradation of water contaminants in other AOPs different from photocatalysis [110], as presented in Figure 8a. Figure 8 shows a depiction of the chemical mechanism that produces these reactant species over two types of nanoparticles involved in different AOPs, resulting in the final degradation of pollutants into carbon dioxide and water.

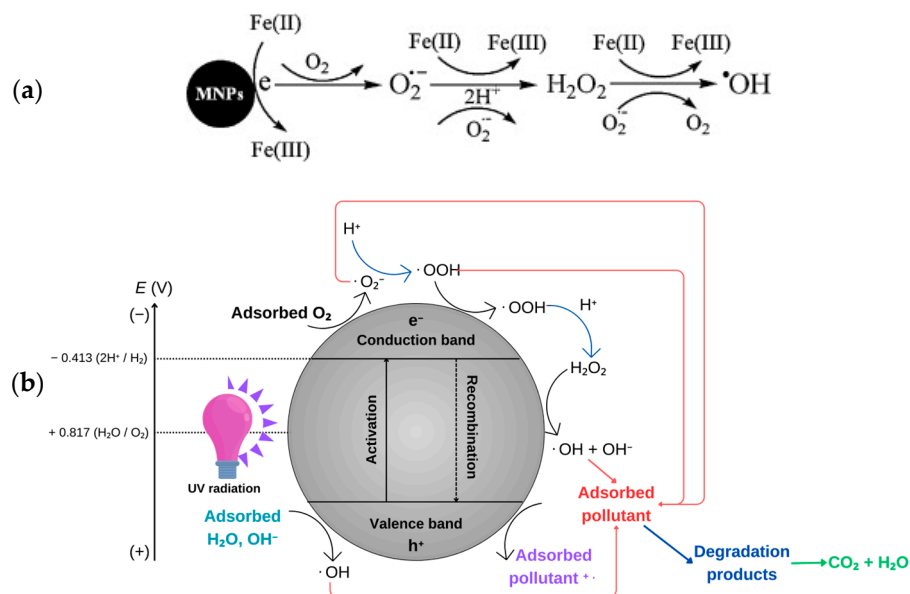


**Figure 8.** Mechanism of generation of reactive species O<sub>2</sub><sup>•-</sup> and •OH in AOPs using (a) iron oxide nanoparticles and (b) TiO<sub>2</sub> nanoparticles. Reprinted with permission from [110]: (a) copyright 2013 and adapted with permission from [111]: (b) copyright 2016 Elsevier.

On the photocatalytic degradation of violet dye using iron oxide nanoparticles (IONPs), Yassin et al. found that the removal efficiency of violet dye was concentration and time dependent, reaching a peak of 99.23% after 210 min of sunlight exposure [112]. Additionally, the green-based synthesis of IONPs in this study demonstrated relevant associated antioxidant activity, further emphasizing their potential in environmentally friendly approaches for eliminating industrial synthetic dyes and remediating contaminated environments and aquatic ecosystems. Regarding the photocatalytic removal of mono-, di-, and tri-nitrophenols from water, Rao et al. synthesized a nano-Fe<sub>3</sub>O<sub>4</sub>-loaded chitosan salicylamide copper (CSC) complex and investigated its photocatalytic properties under sunlight [113]. The methodology involved the preparation and characterization of the composite material using techniques such as spectroscopy and microscopy. The water treatment methodology involved maintaining an acid solution of pH 2.5, a catalyst dose of 50 mg/L, and an initial concentration of nitrophenols of 200 mg/L under sunlight for 60 min. Their experimental data confirmed the successful degradation of mono-nitrophenol and di-nitrophenol within 30 min and tri-nitrophenol within 25 min. This study provided valuable insights into the time-dependent efficacy of the IONP-loaded CSC composite for the degradation of nitrophenols.

The magnetic core of the materials (for single SPIONs or their agglomerates [114,115]) allows them to be easily separated from the treated water using a magnet arrangement, making the process efficient and the particles reusable. In this sense, several authors [116–119] have collectively discussed and highlighted the use of iron oxides (Fe<sub>3</sub>O<sub>4</sub> and γ-Fe<sub>2</sub>O<sub>3</sub>) as the magnetic component in titanium-based photocatalysts. Overall, these nanocomposites have been able to achieve a high photocatalytic efficiency in the removal of dyes from water media under ultraviolet (UV) light exposure [19]. However, limitations exist regarding the use of MNPCs; most common materials (i.e., TiO<sub>2</sub> and ZnO) have the current limitation of

only being stimulated by photons near the UV region, which corresponds to only approximately 5% of the solar spectrum, thereby restricting the use of solar energy [100]. Another limitation of using titanium-based nanophotocatalysts was pointed out by Gopinath et al., who asserted that the application of TiO<sub>2</sub> in industrial-scale wastewater treatment faces serious challenges due to the considerable cost associated with TiO<sub>2</sub> as a raw material, coupled with the inherent problems in preparing nanostructures and composites based on it [120]. Additionally, the process involves high energy requirements, particularly in the provision of UV light.

Future efforts in the development of MNPCs should focus on optimizing their composition toward enhancing their responsiveness to a broader spectrum of solar radiation. While the integration of iron-based components within TiO<sub>2</sub> structures has proven efficient in achieving high photocatalytic efficiency for dye removal under UV light, the challenge lies in expanding their range to harness a larger portion of the solar spectrum. Future research may explore novel magnetic materials and innovative compositions to extend the capabilities of MNPCs into visible light wavelengths. A last limitation is environment-related, since among the various types of nanophotocatalysts that have been proven to be successful agents to remove pollutants from water, only ZnO stands out as a generally accepted environmentally safe metal oxide [109,121]. Finally, the utilization of MNPCs exhibits significant potential; yet, their application is presently limited, necessitating targeted research endeavors to enhance process design and efficient scale-up.

Concerning the physical structure and configuration of the material, even though it is known that reducing the particle size enhances the contaminant adsorption/degradation capacity and the material's reactivity in either adsorption or AOPs, it simultaneously poses challenges concerning recovery, stability, and potential toxicity [122]. To address these constraints associated with SPIONs for environmental remediation, hybrid nanocomposites have been developed by embedding or overlaying fine particles onto larger solid polymeric structures [98,108], resulting in a magnetic nanocomposite rooted in a polymer matrix. Magnetic polymeric nanocomposites can be produced through the deposition of SPIONs onto porous membranes or via their integration with polymeric or inorganic membranes [123], which can be later used for water filtration. When it comes to the latter, a predominant drawback encountered with many conventional membrane materials is fouling. Fouling has the detrimental effect of diminishing flux in output streams and compromising the quality of the permeate, ultimately increasing operational costs [124]. The incorporation of metal oxide SPIONs into membrane fabrication has emerged as a promising strategy to enhance permeability and resistance to fouling, ultimately elevating the quality of the permeate. Indeed, researchers have explored the integration of iron oxide MNPs into membrane matrices as a viable approach to enhance their performance characteristics and mitigate fouling issues [125,126]. One example of this type of application involved the synthesis of magnetic Fe<sub>3</sub>O<sub>4</sub>/graphene oxide (MGO) particles using a simple one-step chemical coprecipitation method [127]. These particles were then introduced into a polyvinylidene fluoride (PVDF) casting solution. Through magnetophoresis, the MGO sheets migrated directionally and arranged in an orderly manner. This unique structure significantly improved the pure water flux, hydrophilicity, and antifouling properties of the membranes. Another example of the use of magnetophoresis to improve membrane structures is the study carried out by Tang et al., which explored the enhancement in proton conductivity in ionomer membranes through the application of a magnetic field during fabrication [128].

Finally, the removal of nano- and microplastics represents a significant and contemporary environmental challenge that has garnered increasing attention in the field of environmental science and engineering [129]. Nanoplastics, a term that encompasses all polymer particles smaller than one micrometer in size, can vary in their definition and are recognized as a newly emerging contaminant [99]. They have now become widespread in natural water environments, presenting a risk to both aquatic ecosystems and human health. Although the current scientific understanding of nano- and microplastics is currently

constrained, conventional water treatment techniques (e.g., coagulation, filtration, etc.) frequently demonstrate limited efficiency and effectiveness for the removal of microplastics. Notably, adsorption technology has lately gained significant attention due to its capability to capture nano- and microplastics, yielding remarkable removal efficiency [130]. The latest discoveries in utilizing SPIONs as adsorbents for the magnetic retrieval of nano- and microplastics show that magnetic separation methods have the potential to be a promising solution for dealing with the urgent worldwide issue of extracting these pollutants from water. Although their use for the removal of nano- and microplastics is still limited to a small number of studies, recent results are promising. Sarcletti et al. developed a novel material, nanoplastic-capturing SPIONs, which allows for the adjustment of the nanoparticle surface charge, ranging from positive to negative, by utilizing corresponding phosphonic acid monolayers [99]. It was observed that their SPIONs possessed the capability to attract (and aggregate with) oppositely charged nanoplastic debris, regardless of their distinct chemical compositions and sizes. These SPION–nanoplastic agglomerates could be efficiently removed from water through magnetophoresis. Furthermore, the study showed that mixtures of nanoplastics with different surface charges could be effectively removed using their particles. More recently, Yan et al. investigated the influence of the water pH and salinity on the efficiency of microplastic removal using magnetic  $\text{Fe}_3\text{O}_4$  nanoparticles [131]. The findings indicated that iron oxide nanoparticles were successful in removing a substantial portion (up to 92.9%) of microplastics within a one-hour timeframe. Additionally, the aggregation dynamics of these particles were notably impacted by pH-related electrostatic forces. This influence encompassed electrostatic attraction and charge neutralization in acidic conditions, as well as electrostatic repulsion under alkaline conditions. Consequently, these pH-induced variations had a marked effect on the effectiveness of microplastic removal. Concerning salinity, it was observed that higher levels promoted the self-aggregation of pollutants. This process diminished the electrostatic repulsion between functionalized SPIONs and microplastics in alkaline conditions, ultimately enhancing the efficiency of the process. Shi et al. experimented with the removal of polyethylene, polypropylene, polystyrene, and polyethylene terephthalate particles using functionalized  $\text{Fe}_3\text{O}_4$  commercial nanoparticles [132]. Through surface adsorption and magnetic separation, the researchers obtained an average removal rate of 80% across the different types of microplastics involved within 150 min. The rate of removal showed variability depending on the type of polymer and size of microplastics, with a positive correlation observed with the amount of  $\text{Fe}_3\text{O}_4$  nanoparticles collated to the microplastic surfaces. The promising results of this study involved the removal of microplastics in simulated seawater, which was notably higher when compared to pure water. Furthermore, their method proved to be highly effective in removing microplastics from various environmental water sources, including river water, domestic sewage, and natural seawater, achieving removal rates exceeding 80%.

These studies are instances of the recent successful use of SPIONs as adsorbents for the removal of nano- and microplastics from water. Regarding the potential drawbacks of this technology, Gao et al. highlighted that, despite being proven as an efficient and simple removal process, adsorption and magnetic separation of microplastics might cause additional pollution and this issue needs to be further explored. In contrast, Zoppas et al. [133], through a comprehensive analysis of the current panorama of microplastic removal from water, recommended the investigation of frameworks that focus on the integration of various types of treatments (physical, chemical, and biological) to achieve high separation/removal efficiencies while minimally compromising the environmental aspect. In summary, SPIONs have demonstrated exceptional efficiency in removing contaminants, such as heavy metals, organic pollutants, and pathogens, from water sources via AOPs and adsorption, as well as integrated into novel membranes employed in water filtration processes.

Finally, Table 3 brings a collection of relevant environmental remediation realizations regarding the use of SPIONs in water media from the last five years. These combined advancements showcase the multifaceted potential of SPIONs in addressing the press-

ing challenges of global water pollution and offer promising prospects for sustainable environmental remediation strategies.

**Table 3.** Collection of recent studies using SPIONs for environmental remediation.

Particle Composition Size (nm)	Magnetic Particle/Composite	Application	Target Species	Matrix	Ref.
Fe <sub>3</sub> O <sub>4</sub> 27.9	Biocomposite obtained from raffia fibers, Fe <sub>3</sub> O <sub>4</sub> nanoparticles and <i>Lindnera jadinii</i> yeast.	Biological adsorbent	Cd(II) ions	Water	[134]
Fe <sub>3</sub> O <sub>4</sub> 31	Polyethyleneimine-functionalized magnetite nanoparticles (PEI-MNPs).	Recovery and regeneration	Fucoidan	Water	[135]
Fe <sub>3</sub> O <sub>4</sub> 80–100	Cobalt-doped Fe <sub>3</sub> O <sub>4</sub> encapsulated with a zirconium-based metal–organic framework.	Removal and adsorption	Fenitrothion (removed) and phosphate (adsorbed)	Water	[136]
Fe <sub>3</sub> O <sub>4</sub> -	Fe <sub>3</sub> O <sub>4</sub> loaded on persimmon tannin-functionalized (Ti <sub>3</sub> C <sub>2</sub> -NH <sub>2</sub> ) composite.	Removal via adsorption	U(VI) and Cr(VI) ions	Water	[137]
Fe <sub>3</sub> O <sub>4</sub> 15	Uniformly distributed with a composition of 77.02% and 48.56% of Fe before and after the Fenton process, respectively.	Reduction in chemical oxygen demand (COD)	COD removal	Landfill leachate	[138]
Fe <sub>3</sub> O <sub>4</sub> -	Superparamagnetic Fe <sub>3</sub> O <sub>4</sub> ( $M = 23.13$ emu/g) and magnetite-olive pomace nanocomposite ( $M = 16.15$ emu/g).	Removal through sorption	Ce(III)	Water	[139]
Fe <sub>3</sub> O <sub>4</sub> 20	Uniformly distributed, superparamagnetic Fe <sub>3</sub> O <sub>4</sub> functionalized with <i>Moringa eleifera</i> salt extract ( $M = 63$ emu/g).	Removal through magnetic coagulation	Tartrazine yellow dye	Wastewater	[140]
Fe <sub>3</sub> O <sub>4</sub> 25	Fe <sub>3</sub> O <sub>4</sub> with a magnetic chitosan shell coated with polyaniline.	Removal via adsorption and reduction	Cr(VI)	Wastewater	[141]
Fe <sub>3</sub> O <sub>4</sub> 160	Superparamagnetic Fe <sub>3</sub> O <sub>4</sub> ( $M = 52.6$ emu/g) and Fe <sub>3</sub> O <sub>4</sub> @COF <sup>1</sup> composites ( $M = 48.4$ emu/g).	Removal via adsorption and magnetic extraction	Triclosan and triclocarban	Water	[142]
Fe <sub>3</sub> O <sub>4</sub> 5–10	TiO <sub>2</sub> -graphene oxide-Fe <sub>3</sub> O <sub>4</sub> nanocomposite.	Degradation through photo-Fenton process	Amoxicillin	Wastewater	[143]

<sup>1</sup> Covalent Organic Framework.

## 5. Conclusions

SPIONs have gained significant attention due to their magnetic properties and bio-compatible coatings, making them applicable in various fields. SPIONs can be manipulated through the use of magnetic field gradients, a process recognized as magnetophoresis, thereby offering an efficient means of separating targeted components from liquid media for several biomedical and chemical engineering applications. Magnetic separation surpasses conventional methods employed for the recovery of particulate material from liquids in terms of precision, swiftness, process duration, and efficiency, as well as cost, making it a promising technique for various applications.

Two magnetic separation techniques, HGMS and LGMS, have emerged as focal methods for the isolation and retrieval of SPIONs. HGMS entails the deployment of packed columns replete with a ferromagnetic material to trap magnetic particles, proffering a high separation efficiency and the capability to recover even the smallest SPIONs. Noteworthy commercial implementations of this technology, such as the MACS system developed by Miltenyi Biotech, prove its practical utility. Nevertheless, HGMS is, among other factors, mainly limited by the potential non-specific particle capture and the potential for the permanent entrapment of SPIONs. On the other hand, LGMS is offered as a cost-effective alternative, depending on lower magnetic gradients and simpler configurations. It is particularly suited for applications within the biological fields, where magnetic nanoparticles are exploited for the precise sorting and assessment of targeted biomolecules and cell populations. However, LGMS is confronted with challenges from the lower magnetic forces acting on the SPIONs, thus increasing the duration of the separation process.

SPIONs can be used in diverse applications across a multitude of fields. This type of nanoparticle plays an important role in targeted drug delivery, characterized by the specialized functionalization and controlled release of therapeutic agents at specified sites, facilitated by external magnetic fields. This approach minimizes undesirable side effects

and diminishes the required dosage of pharmaceuticals. For magnetic cell separation, SPIONs, when conjugated with antibodies, enable the isolation of specific cell types from heterogeneous populations, particularly stem cells and cancer cells from complex biofluid samples. For environmental remediation, SPIONs play a pivotal role in the removal of contaminants from water systems, including heavy metals, organic compounds, as well as nano- and microplastics, thereby offering sustainable solutions to solve environmental challenges encountered in water treatment plants.

**Author Contributions:** Conceptualization, X.W. and S.C.; methodology, J.G.-P.; formal analysis, H.C.; investigation, X.W.; resources, H.C.; data curation, H.C. and J.S.; writing—original draft preparation, X.W., S.C. and J.G.-P.; writing—review and editing, K.W. and J.C.; supervision, K.W., J.C. and J.G.-P.; project administration, J.G.-P.; funding acquisition, J.C. and J.G.-P. All authors have read and agreed to the published version of the manuscript.

**Funding:** This research was funded by Texas Tech University through HEF New Faculty Startup, NRUF Startup and Core Research Support Fund. We also wish to thank the National Heart, Lung, and Blood Institute (1R01HL131720-01A1) and DARPA (BAA07-21) for financial assistance.

**Data Availability Statement:** Data are contained within the article.

**Conflicts of Interest:** The authors declare no conflict of interest.

## References

1. Laurent, S.; Forge, D.; Port, M.; Roch, A.; Robic, C.; Vander Elst, L.; Muller, R.N. Magnetic iron oxide nanoparticles: Synthesis, stabilization, vectorization, physicochemical characterizations, and biological applications. *Chem. Rev.* **2008**, *108*, 2064–2110. [[CrossRef](#)]
2. Buzea, C.; Pacheco, I.I.; Robbie, K. Nanomaterials and nanoparticles: Sources and toxicity. *Biointerphases* **2007**, *2*, MR17–MR71. [[CrossRef](#)]
3. Rezaei, B.; Yari, P.; Sanders, S.M.; Wang, H.; Chugh, V.K.; Liang, S.; Mostufa, S.; Xu, K.; Wang, J.P.; Gómez-Pastora, J. Magnetic Nanoparticles: A Review on Synthesis, Characterization, Functionalization, and Biomedical Applications. *Small* **2023**, e2304848. [[CrossRef](#)]
4. Mitchell, M.J.; Billingsley, M.M.; Haley, R.M.; Wechsler, M.E.; Peppas, N.A.; Langer, R. Engineering precision nanoparticles for drug delivery. *Nat. Rev. Drug Discov.* **2021**, *20*, 101–124. [[CrossRef](#)]
5. Kaur, P.; Aliru, M.L.; Chadha, A.S.; Asea, A.; Krishnan, S. Hyperthermia using nanoparticles—promises and pitfalls. *Int. J. Hyperth.* **2016**, *32*, 76–88. [[CrossRef](#)]
6. Estelrich, J.; Sánchez-Martín, M.J.; Busquets, M.A. Nanoparticles in magnetic resonance imaging: From simple to dual contrast agents. *Int. J. Nanomed.* **2015**, *10*, 1727–1741.
7. Hans, M.L.; Lowman, A.M. Biodegradable nanoparticles for drug delivery and targeting. *Curr. Opin. Solid State Mater. Sci.* **2002**, *6*, 319–327. [[CrossRef](#)]
8. Wu, L.; Mendoza-Garcia, A.; Li, Q.; Sun, S. Organic phase syntheses of magnetic nanoparticles and their applications. *Chem. Rev.* **2016**, *116*, 10473–10512. [[CrossRef](#)]
9. Frenkel, J.; Doefman, J. Spontaneous and induced magnetisation in ferromagnetic bodies. *Nature* **1930**, *126*, 274–275. [[CrossRef](#)]
10. Gómez-Pastora, J.; Bringas, E.; Ortiz, I. Recent progress and future challenges on the use of high performance magnetic nano-adsorbents in environmental applications. *Chem. Eng. J.* **2014**, *256*, 187–204. [[CrossRef](#)]
11. Gómez-Pastora, J.; Bringas, E.; Lázaro-Díez, M.; Ramos-Vivas, J.; Ortiz, I. The reverse of controlled release: Controlled sequestration of species and biotoxins into nanoparticles (NPs). In *Drug Delivery Systems*; Stroeve, P., Mahmoudi, M., Eds.; World Scientific Publishing: Singapore, 2018; pp. 207–244.
12. Yavuz, C.T.; Prakash, A.; Mayo, J.; Colvin, V.L. Magnetic separations: From steel plants to biotechnology. *Chem. Eng. Sci.* **2009**, *64*, 2510–2521. [[CrossRef](#)]
13. Friedman, G.; Yellen, B. Magnetic separation, manipulation and assembly of solid phase in fluids. *Curr. Opin. Colloid Interface Sci.* **2005**, *10*, 158–166. [[CrossRef](#)]
14. Gijs, M.A.; Lacharme, F.; Lehmann, U. Microfluidic applications of magnetic particles for biological analysis and catalysis. *Chem. Rev.* **2010**, *110*, 1518–1563. [[CrossRef](#)] [[PubMed](#)]
15. Hoshier, A.K.; Le, T.-A.; Valdastrì, P.; Yoon, J. Swarm of magnetic nanoparticles steering in multi-bifurcation vessels under fluid flow. *J. Micro. Bio. Rob.* **2020**, *16*, 137–145. [[CrossRef](#)]
16. Gong, D.; Celi, N.; Zhang, D.; Cai, J. Magnetic biohybrid microrobot multimers based on chlorella cells for enhanced targeted drug delivery. *ACS Appl. Mater. Interfaces* **2022**, *14*, 6320–6330. [[CrossRef](#)]
17. Li, X.; Yue, R.; Guan, G.; Zhang, C.; Zhou, Y.; Song, G. Recent development of pH-responsive theranostic nanoplatfoms for magnetic resonance imaging-guided cancer therapy. *Exploration* **2023**, *3*, 20220002. [[CrossRef](#)]

18. Gómez-Pastora, J.; Xue, X.; Karampelas, I.H.; Bringas, E.; Furlani, E.P.; Ortiz, I. Analysis of separators for magnetic beads recovery: From large systems to multifunctional microdevices. *Sep. Purif. Technol.* **2017**, *172*, 16–31. [[CrossRef](#)]
19. Gómez-Pastora, J.; Dominguez, S.; Bringas, E.; Rivero, M.J.; Ortiz, I.; Dionysiou, D.D. Review and perspectives on the use of magnetic nanophotocatalysts (MNPCs) in water treatment. *Chem. Eng. J.* **2017**, *310*, 407–427. [[CrossRef](#)]
20. Waifalkar, P.; Parit, S.; Chougale, A.; Sahoo, S.C.; Patil, P.; Patil, P. Immobilization of invertase on chitosan coated  $\gamma$ -Fe<sub>2</sub>O<sub>3</sub> magnetic nanoparticles to facilitate magnetic separation. *J. Colloid Interface Sci.* **2016**, *482*, 159–164. [[CrossRef](#)] [[PubMed](#)]
21. Samrot, A.V.; Sahithya, C.S.; Selvarani, J.; Purayil, S.K.; Ponnaiah, P. A review on synthesis, characterization and potential biological applications of superparamagnetic iron oxide nanoparticles. *Curr. Res. Green Sustain. Chem.* **2021**, *4*, 100042. [[CrossRef](#)]
22. Yari, P.; Liang, S.; Chugh, V.K.; Rezaei, B.; Mostufa, S.; Krishna, V.D.; Saha, R.; Cheeran, M.C.-J.; Wang, J.-P.; Gómez-Pastora, J. Nanomaterial-Based Biosensors for SARS-CoV-2 and Future Epidemics. *Anal. Chem.* **2023**, *42*, 15419–15449. [[CrossRef](#)]
23. Gaß, H.; Sarcletti, M.; Müller, L.; Hübner, S.; Yokosawa, T.; Park, H.; Przybilla, T.; Spiecker, E.; Halik, M. A Sustainable Method for Removal of the Full Range of Liquid and Solid Hydrocarbons from Water Including Up-and Recycling. *Adv. Sci.* **2023**, *10*, 2302495. [[CrossRef](#)]
24. Furlani, E.P. Magnetic biotransport: Analysis and applications. *Materials* **2010**, *3*, 2412–2446. [[CrossRef](#)]
25. Mostufa, S.; Rezaei, B.; Yari, P.; Xu, K.; Gómez-Pastora, J.; Sun, J.; Shi, Z.; Wu, K. Giant Magnetoresistance Based Biosensors for Cancer Screening and Detection. *ACS Appl. Bio Mater.* **2023**, *6*, 4042–4059. [[CrossRef](#)]
26. Richardson, O.W. A mechanical effect accompanying magnetization. *Phys. Rev.* **1908**, *26*, 248. [[CrossRef](#)]
27. Stoner, E.C.; Wohlfarth, E. A mechanism of magnetic hysteresis in heterogeneous alloys. *Philos. Trans. R. Soc. A* **1948**, *240*, 599–642. [[CrossRef](#)]
28. Zborowski, M.; Chalmers, J.J.; Lowrie, W.G. Magnetic Cell Manipulation and Sorting. In *Microtechnology for Cell Manipulation and Sorting*; Lee, W., Tseng, P., Di Carlo, D., Eds.; Springer International Publishing: Cham, Switzerland, 2017; pp. 15–55.
29. De Las Cuevas, G.; Faraudo, J.; Camacho, J. Low-Gradient Magnetophoresis through Field-Induced Reversible Aggregation. *J. Phys. Chem. C* **2008**, *112*, 945–950. [[CrossRef](#)]
30. Gómez-Pastora, J.; Wu, X.; Sundar, N.; Alawi, J.; Nabar, G.; Winter, J.O.; Zborowski, M.; Chalmers, J.J. Self-assembly and sedimentation of 5 nm SPIONs using horizontal, high magnetic fields and gradients. *Sep. Purif. Technol.* **2020**, *248*, 117012. [[CrossRef](#)] [[PubMed](#)]
31. Leong, S.S.; Ahmad, Z.; Lim, J. Magnetophoresis of superparamagnetic nanoparticles at low field gradient: Hydrodynamic effect. *Soft Matter* **2015**, *11*, 6968–6980. [[CrossRef](#)] [[PubMed](#)]
32. Leong, S.S.; Ahmad, Z.; Camacho, J.; Faraudo, J.; Lim, J. Kinetics of low field gradient magnetophoresis in the presence of magnetically induced convection. *J. Phys. Chem. C* **2017**, *121*, 5389–5407. [[CrossRef](#)]
33. Moeser, G.D.; Roach, K.A.; Green, W.H.; Alan Hatton, T.; Laibinis, P.E. High-gradient magnetic separation of coated magnetic nanoparticles. *AIChE J.* **2004**, *50*, 2835–2848. [[CrossRef](#)]
34. Ge, W.; Encinas, A.; Araujo, E.; Song, S. Magnetic matrices used in high gradient magnetic separation (HGMS): A review. *Results Phys.* **2017**, *7*, 4278–4286. [[CrossRef](#)]
35. Wu, X.; Gómez-Pastora, J.; Zborowski, M.; Chalmers, J. SPIONs self-assembly and magnetic sedimentation in quadrupole magnets: Gaining insight into the separation mechanisms. *Sep. Purif. Technol.* **2022**, *280*, 119786. [[CrossRef](#)] [[PubMed](#)]
36. Miltenyi, S.; Müller, W.; Weichel, W.; Radbruch, A. High gradient magnetic cell separation with MACS. *Cytom. J. Int. Soc. Anal. Cytol.* **1990**, *11*, 231–238. [[CrossRef](#)] [[PubMed](#)]
37. Podoynitsyn, S.N.; Sorokina, O.N.; Kovarski, A.L. High-gradient magnetic separation using ferromagnetic membrane. *J. Magn. Mater.* **2016**, *397*, 51–56. [[CrossRef](#)]
38. González Fernández, C.; Gómez Pastora, J.; Basauri, A.; Fallanza, M.; Bringas, E.; Chalmers, J.J.; Ortiz, I. Continuous-flow separation of magnetic particles from biofluids: How does the microdevice geometry determine the separation performance? *Sensors* **2020**, *20*, 3030. [[CrossRef](#)]
39. Zborowski, M.; Sun, L.; Moore, L.R.; Williams, P.S.; Chalmers, J.J. Continuous cell separation using novel magnetic quadrupole flow sorter. *J. Magn. Mater.* **1999**, *194*, 224–230. [[CrossRef](#)]
40. Schaller, V.; Kräling, U.; Rusu, C.; Petersson, K.; Wipenmyr, J.; Krozer, A.; Wahnström, G.; Sanz-Velasco, A.; Enoksson, P.; Johansson, C. Motion of nanometer sized magnetic particles in a magnetic field gradient. *J. Appl. Phys.* **2008**, *104*, 093918. [[CrossRef](#)]
41. Williams, P.S.; Zborowski, M.; Chalmers, J.J. Flow rate optimization for the quadrupole magnetic cell sorter. *Anal. Chem.* **1999**, *71*, 3799–3807. [[CrossRef](#)]
42. Jing, Y.; Moore, L.R.; Williams, P.S.; Chalmers, J.J.; Farag, S.S.; Bolwell, B.; Zborowski, M. Blood progenitor cell separation from clinical leukapheresis product by magnetic nanoparticle binding and magnetophoresis. *Biotechnol. Bioeng.* **2007**, *96*, 1139–1154. [[CrossRef](#)]
43. Moore, L.R.; Nehl, F.; Dorn, J.; Chalmers, J.J.; Zborowski, M. Open gradient magnetic red blood cell sorter evaluation on model cell mixtures. *IEEE Trans. Magn.* **2013**, *49*, 309–315. [[CrossRef](#)] [[PubMed](#)]
44. González-Fernández, C.; Gómez-Pastora, J.; Bringas, E.; Zborowski, M.; Chalmers, J.J.; Ortiz, I. Recovery of magnetic catalysts: Advanced design for process intensification. *Ind. Eng. Chem. Res.* **2021**, *60*, 16780–16790. [[CrossRef](#)] [[PubMed](#)]
45. Leong, S.S.; Ahmad, Z.; Low, S.C.; Camacho, J.; Faraudo, J.; Lim, J. Unified View of Magnetic Nanoparticle Separation under Magnetophoresis. *Langmuir* **2020**, *36*, 8033–8055. [[CrossRef](#)] [[PubMed](#)]

46. Medvedeva, I.; Bakhteeva, Y.; Zhakov, S.; Revvo, A.; Byzov, I.; Uimin, M.; Yermakov, A.; Mysik, A. Sedimentation and aggregation of magnetite nanoparticles in water by a gradient magnetic field. *J. Nanopart. Res.* **2013**, *15*, 2054. [[CrossRef](#)]
47. Yeap, S.P.; Leong, S.S.; Ahmad, A.L.; Ooi, B.S.; Lim, J. On size fractionation of iron oxide nanoclusters by low magnetic field gradient. *J. Phys. Chem. C* **2014**, *118*, 24042–24054. [[CrossRef](#)]
48. Bakhteeva, I.A.; Medvedeva, I.; Uimin, M.; Byzov, I.; Zhakov, S.; Yermakov, A.; Shchegoleva, N. Magnetic sedimentation and aggregation of Fe<sub>3</sub>O<sub>4</sub>@SiO<sub>2</sub> nanoparticles in water medium. *Sep. Purif. Technol.* **2016**, *159*, 35–42. [[CrossRef](#)]
49. Lim, J.; Yeap, S.P.; Low, S.C. Challenges associated to magnetic separation of nanomaterials at low field gradient. *Sep. Purif. Technol.* **2014**, *123*, 171–174. [[CrossRef](#)]
50. Faraudo, J.; Camacho, J. Cooperative magnetophoresis of superparamagnetic colloids: Theoretical aspects. *Colloid Polym. Sci.* **2010**, *288*, 207–215. [[CrossRef](#)]
51. Faraudo, J.; Andreu, J.S.; Calero, C.; Camacho, J. Predicting the Self-Assembly of Superparamagnetic Colloids under Magnetic Fields. *Adv. Funct. Mater.* **2016**, *26*, 3837–3858. [[CrossRef](#)]
52. Andreu, J.; Camacho, J.; Faraudo, J.; Benelmekki, M.; Rebollo, C.; Martínez, L.M. Simple analytical model for the magnetophoretic separation of superparamagnetic dispersions in a uniform magnetic gradient. *Phys. Rev. E* **2011**, *84*, 021402. [[CrossRef](#)]
53. Alves, M.N.; Miró, M.; Breadmore, M.C.; Macka, M. Trends in analytical separations of magnetic (nano)particles. *TrAC Trends Anal. Chem.* **2019**, *114*, 89–97. [[CrossRef](#)]
54. Furlani, E.P. Analysis of particle transport in a magnetophoretic microsystem. *J. Appl. Phys.* **2006**, *99*, 024912. [[CrossRef](#)]
55. Pamme, N. On-chip bioanalysis with magnetic particles. *Curr. Opin. Chem. Biol.* **2012**, *16*, 436–443. [[CrossRef](#)] [[PubMed](#)]
56. Yeap, S.P.; Ahmad, A.L.; Ooi, B.S.; Lim, J. Electrosteric stabilization and its role in cooperative magnetophoresis of colloidal magnetic nanoparticles. *Langmuir* **2012**, *28*, 14878–14891. [[CrossRef](#)]
57. Toh, P.Y.; Ng, B.W.; Ahmad, A.L.; Chieh, D.C.J.; Lim, J. Magnetophoretic separation of *Chlorella* sp.: Role of cationic polymer binder. *Process Saf. Environ. Prot.* **2014**, *92*, 515–521. [[CrossRef](#)]
58. Pamme, N.; Wilhelm, C. Continuous sorting of magnetic cells via on-chip free-flow magnetophoresis. *Lab Chip* **2006**, *6*, 974–980. [[CrossRef](#)]
59. Tong, S.; Zhu, H.; Bao, G. Magnetic iron oxide nanoparticles for disease detection and therapy. *Mater. Today* **2019**, *31*, 86–99. [[CrossRef](#)] [[PubMed](#)]
60. Xu, H.; Aguilar, Z.P.; Yang, L.; Kuang, M.; Duan, H.; Xiong, Y.; Wei, H.; Wang, A. Antibody conjugated magnetic iron oxide nanoparticles for cancer cell separation in fresh whole blood. *Biomaterials* **2011**, *32*, 9758–9765. [[CrossRef](#)]
61. Lin, J.; Li, M.; Li, Y.; Chen, Q. A high gradient and strength bioseparator with nano-sized immunomagnetic particles for specific separation and efficient concentration of *E. coli* O157: H7. *J. Magn. Magn. Mater.* **2015**, *378*, 206–213. [[CrossRef](#)]
62. Leong, S.S.; Yeap, S.P.; Lim, J. Working principle and application of magnetic separation for biomedical diagnostic at high-and low-field gradients. *Interface Focus* **2016**, *6*, 20160048. [[CrossRef](#)]
63. Ciannella, S.; Wu, X.; González-Fernández, C.; Rezaei, B.; Strayer, J.; Choe, H.; Wu, K.; Chalmers, J.; Gomez-Pastora, J. Kinetic and Parametric Analysis of the Separation of Ultra-Small, Aqueous Superparamagnetic Iron Oxide Nanoparticle Suspensions under Quadrupole Magnetic Fields. *Micromachines* **2023**, *14*, 2107. [[CrossRef](#)]
64. Ali, A.; Shah, T.; Ullah, R.; Zhou, P.; Guo, M.; Ovais, M.; Tan, Z.; Rui, Y. Review on Recent Progress in Magnetic Nanoparticles: Synthesis, Characterization, and Diverse Applications. *Front. Chem.* **2021**, *9*, 629054. [[CrossRef](#)] [[PubMed](#)]
65. Wagner, V.; Dullaart, A.; Bock, A.-K.; Zweck, A. The emerging nanomedicine landscape. *Nat. Biotechnol.* **2006**, *24*, 1211–1217. [[CrossRef](#)] [[PubMed](#)]
66. Freeman, M.; Arrott, A.; Watson, J. Magnetism in medicine. *J. Appl. Phys.* **1960**, *31*, S404–S405. [[CrossRef](#)]
67. Senyei, A.; Widder, K.; Czerlinski, G. Magnetic guidance of drug-carrying microspheres. *J. Appl. Phys.* **1978**, *49*, 3578–3583. [[CrossRef](#)]
68. Senyei, A.E.; Widder, K.J.; Reich, S.D.; Gonczy, C. In vivo kinetics of magnetically targeted low-dose doxorubicin. *J. Pharm. Sci.* **1981**, *70*, 389–391. [[CrossRef](#)]
69. Lübbe, A.S.; Bergemann, C.; Huhnt, W.; Fricke, T.; Riess, H.; Brock, J.W.; Huhn, D. Preclinical experiences with magnetic drug targeting: Tolerance and efficacy. *Cancer Res.* **1996**, *56*, 4694–4701.
70. Nasongkla, N.; Bey, E.; Ren, J.; Ai, H.; Khemtong, C.; Guthi, J.S.; Chin, S.-F.; Sherry, A.D.; Boothman, D.A.; Gao, J. Multifunctional polymeric micelles as cancer-targeted, MRI-ultrasensitive drug delivery systems. *Nano. Lett.* **2006**, *6*, 2427–2430. [[CrossRef](#)]
71. Neuberger, T.; Schöpf, B.; Hofmann, H.; Hofmann, M.; Von Rechenberg, B. Superparamagnetic nanoparticles for biomedical applications: Possibilities and limitations of a new drug delivery system. *J. Magn. Magn. Mater.* **2005**, *293*, 483–496. [[CrossRef](#)]
72. Lübbe, A.S.; Alexiou, C.; Bergemann, C. Clinical applications of magnetic drug targeting. *J. Surg. Res.* **2001**, *95*, 200–206. [[CrossRef](#)]
73. Gupta, A.K.; Naregalkar, R.R.; Vaidya, V.D.; Gupta, M. Recent advances on surface engineering of magnetic iron oxide nanoparticles and their biomedical applications. *Nanomedicine* **2007**, *2*, 23–39. [[CrossRef](#)]
74. Santhosh, P.B.; Ulrih, N.P. Multifunctional superparamagnetic iron oxide nanoparticles: Promising tools in cancer theranostics. *Cancer Lett.* **2013**, *336*, 8–17. [[CrossRef](#)] [[PubMed](#)]
75. Ayubi, M.; Karimi, M.; Abdpour, S.; Rostamizadeh, K.; Parsa, M.; Zamani, M.; Saedi, A. Magnetic nanoparticles decorated with PEGylated curcumin as dual targeted drug delivery: Synthesis, toxicity and biocompatibility study. *Mater. Sci. Eng. C* **2019**, *104*, 109810. [[CrossRef](#)] [[PubMed](#)]

76. Kumar, P.; Agnihotri, S.; Roy, I. Preparation and characterization of superparamagnetic iron oxide nanoparticles for magnetically guided drug delivery. *Int. J. Nanomed.* **2018**, *13*, 43–46. [[CrossRef](#)] [[PubMed](#)]
77. Perillo, E.; Hervé-Aubert, K.; Allard-Vannier, E.; Falanga, A.; Galdiero, S.; Chourpa, I. Synthesis and in vitro evaluation of fluorescent and magnetic nanoparticles functionalized with a cell penetrating peptide for cancer theranosis. *J. Colloid Interface Sci.* **2017**, *499*, 209–217. [[CrossRef](#)]
78. Zhang, W.; Taheri-Ledari, R.; Hajizadeh, Z.; Zolfaghari, E.; Ahghari, M.R.; Maleki, A.; Hamblin, M.R.; Tian, Y. Enhanced activity of vancomycin by encapsulation in hybrid magnetic nanoparticles conjugated to a cell-penetrating peptide. *Nanoscale* **2020**, *12*, 3855–3870. [[CrossRef](#)]
79. Qian, X.; Yin, R.; Gu, Y.; Zhang, H.; Zhang, W. Drug-attached magnetic nanoparticles: Locomotion control and in vivo biocompatibility. *J. Phys. Conf. Ser.* **2020**, *1549*, 032030. [[CrossRef](#)]
80. Azizi, S.; Nosrati, H.; Danafar, H. Simple surface functionalization of magnetic nanoparticles with methotrexate-conjugated bovine serum albumin as a biocompatible drug delivery vehicle. *Appl. Organomet. Chem.* **2020**, *34*, e5479. [[CrossRef](#)]
81. Nosrati, H.; Sefidi, N.; Sharafi, A.; Danafar, H.; Manjili, H.K. Bovine Serum Albumin (BSA) coated iron oxide magnetic nanoparticles as biocompatible carriers for curcumin-anticancer drug. *Bioorg. Chem.* **2018**, *76*, 501–509. [[CrossRef](#)]
82. Tom, G.; Philip, S.; Isaac, R.; Praseetha, P.; Jiji, S.; Asha, V. Preparation of an efficient and safe polymeric-magnetic nanoparticle delivery system for sorafenib in hepatocellular carcinoma. *Life Sci.* **2018**, *206*, 10–21. [[CrossRef](#)]
83. Cohn, D.; Zarek, M.; Elyashiv, A.; Sbitan, M.A.; Sharma, V.; Ramanujan, R.V. Remotely triggered morphing behavior of additively manufactured thermoset polymer-magnetic nanoparticle composite structures. *Smart Mater. Struct.* **2021**, *30*, 045022. [[CrossRef](#)]
84. Odintsov, B.; Chun, J.L.; Berry, S.E. Whole Body MRI and Fluorescent Microscopy for Detection of Stem Cells Labeled with Superparamagnetic Iron Oxide (SPIO) Nanoparticles and DiI Following Intramuscular and Systemic Delivery. In *Imaging and Tracking Stem Cells: Methods and Protocols*; Turksen, K., Ed.; Humana Press: Totowa, NJ, USA, 2013; pp. 177–193.
85. Petri-Fink, A.; Chastellain, M.; Juillerat-Jeanerret, L.; Ferrari, A.; Hofmann, H. Development of functionalized superparamagnetic iron oxide nanoparticles for interaction with human cancer cells. *Biomaterials* **2005**, *26*, 2685–2694. [[CrossRef](#)] [[PubMed](#)]
86. Shields Iv, C.W.; Reyes, C.D.; López, G.P. Microfluidic cell sorting: A review of the advances in the separation of cells from debulking to rare cell isolation. *Lab Chip* **2015**, *15*, 1230–1249. [[CrossRef](#)] [[PubMed](#)]
87. Karampelas, I.H.; Gómez-Pastora, J. Novel approaches concerning the numerical modeling of particle and cell separation in microchannels: A review. *Processes* **2022**, *10*, 1226. [[CrossRef](#)]
88. Zhou, X.; Luo, B.; Kang, K.; Ma, S.; Sun, X.; Lan, F.; Yi, Q.; Wu, Y. Multifunctional luminescent immuno-magnetic nanoparticles: Toward fast, efficient, cell-friendly capture and recovery of circulating tumor cells. *J. Mater. Chem. B* **2019**, *7*, 393–400. [[CrossRef](#)]
89. Payer, P.; Röder, M.; Camara, O.; Pachmann, K. High depletion of breast cancer cells from the peripheral blood with the method of non-specific separation. *Ecancermedicalscience* **2020**, *14*, 1003. [[CrossRef](#)] [[PubMed](#)]
90. Saei, A.; Asfia, S.; Kouchakzadeh, H.; Rahmandoust, M. Antibody-modified magnetic nanoparticles as specific high-efficient cell-separation agents. *J. Biomed. Mater. Res. Part B* **2020**, *108*, 2633–2642. [[CrossRef](#)] [[PubMed](#)]
91. Unni, M.; Zhang, J.; George, T.J.; Segal, M.S.; Fan, Z.H.; Rinaldi, C. Engineering magnetic nanoparticles and their integration with microfluidics for cell isolation. *J. Colloid Interface Sci.* **2020**, *564*, 204–215. [[CrossRef](#)]
92. Rashid, Z.; Shokri, F.; Abbasi, A.; Khoobi, M.; Zarnani, A.-H. Surface modification and bioconjugation of anti-CD4 monoclonal antibody to magnetic nanoparticles as a highly efficient affinity adsorbent for positive selection of peripheral blood T CD4+ lymphocytes. *Int. J. Biol. Macromol.* **2020**, *161*, 729–737. [[CrossRef](#)]
93. Cai, G.; Wang, S.; Zheng, L.; Lin, J. A fluidic device for immunomagnetic separation of foodborne bacteria using self-assembled magnetic nanoparticle chains. *Micromachines* **2018**, *9*, 624. [[CrossRef](#)]
94. Sahoo, S.L.; Liu, C.-H.; Wu, W.-C. Lymphoma cell isolation using multifunctional magnetic nanoparticles: Antibody conjugation and characterization. *RSC Adv.* **2017**, *7*, 22468–22478. [[CrossRef](#)]
95. Li, C.; Li, Z.; Gan, Y.; Jiang, F.; Zhao, H.; Tan, J.; Yang, Y.Y.; Yuan, P.; Ding, X. Selective Capture, Separation, and Photothermal Inactivation of Methicillin-Resistant Staphylococcus aureus (MRSA) Using Functional Magnetic Nanoparticles. *ACS Appl. Mater. Interfaces* **2022**, *14*, 20566–20575. [[CrossRef](#)] [[PubMed](#)]
96. Rafeeq, H.; Hussain, A.; Ambreen, A.; Waqas, M.; Bilal, M.; Iqbal, H.M. Functionalized nanoparticles and their environmental remediation potential: A review. *J. Nanostruct. Chem.* **2022**, *12*, 1007–1031. [[CrossRef](#)]
97. Tee, G.T.; Gok, X.Y.; Yong, W.F. Adsorption of pollutants in wastewater via biosorbents, nanoparticles and magnetic biosorbents: A review. *Environ. Res.* **2022**, *212*, 113248. [[CrossRef](#)] [[PubMed](#)]
98. Chahar, M.; Khaturia, S.; Singh, H.L.; Solanki, V.S.; Agarwal, N.; Sahoo, D.K.; Yadav, V.K.; Patel, A. Recent advances in the effective removal of hazardous pollutants from wastewater by using nanomaterials—A review. *Front. Environ. Sci.* **2023**, *11*, 1–24. [[CrossRef](#)]
99. Sarcletti, M.; Park, H.; Wirth, J.; Englisch, S.; Eigen, A.; Drobek, D.; Vivod, D.; Friedrich, B.; Tietze, R.; Alexiou, C. The remediation of nano-/microplastics from water. *Mater. Today* **2021**, *48*, 38–46. [[CrossRef](#)]
100. Kim, I.; Yang, H.-M.; Park, C.W.; Yoon, I.-H.; Sihm, Y. (Eds.) Environmental applications of magnetic nanoparticles. In *Magnetic Nanoparticle-Based Hybrid Materials*; Elsevier: Amsterdam, The Netherlands, 2021; pp. 529–545.
101. Doan, L. Modifying Superparamagnetic Iron Oxide Nanoparticles as Methylene Blue Adsorbents: A Review. *ChemEngineering* **2023**, *7*, 77. [[CrossRef](#)]

102. Gutierrez, A.M.; Dziubla, T.D.; Hilt, J.Z. Recent advances on iron oxide magnetic nanoparticles as sorbents of organic pollutants in water and wastewater treatment. *Rev. Environ. Health* **2017**, *32*, 111–117. [[CrossRef](#)]
103. Leonel, A.G.; Mansur, A.A.P.; Mansur, H.S. Advanced Functional Nanostructures based on Magnetic Iron Oxide Nanomaterials for Water Remediation: A Review. *Water Res.* **2021**, *190*, 116693. [[CrossRef](#)]
104. Oladoja, N.A.; Aboluwoye, C.O.; Oladimeji, Y.B.; Ashogbon, A.O.; Otemuyiwa, I.O. Studies on castor seed shell as a sorbent in basic dye contaminated wastewater remediation. *Desalination* **2008**, *227*, 190–203. [[CrossRef](#)]
105. Lin, C.-I.; Wang, L.-H. Rate equations and isotherms for two adsorption models. *J. Chin. Inst. Chem. Eng.* **2008**, *39*, 579–585. [[CrossRef](#)]
106. Hao, Y.-M.; Man, C.; Hu, Z.-B. Effective removal of Cu (II) ions from aqueous solution by amino-functionalized magnetic nanoparticles. *J. Hazard. Mater.* **2010**, *184*, 392–399. [[CrossRef](#)] [[PubMed](#)]
107. Huang, X.; Wang, G.; Yang, M.; Guo, W.; Gao, H. Synthesis of polyaniline-modified Fe<sub>3</sub>O<sub>4</sub>/SiO<sub>2</sub>/TiO<sub>2</sub> composite microspheres and their photocatalytic application. *Mater. Lett.* **2011**, *65*, 2887–2890. [[CrossRef](#)]
108. Khin, M.M.; Nair, A.S.; Babu, V.J.; Murugan, R.; Ramakrishna, S. A review on nanomaterials for environmental remediation. *Energy Environ. Sci.* **2012**, *5*, 8075–8109. [[CrossRef](#)]
109. Abebe, B.; Murthy, H.A.; Amare, E. Summary on adsorption and photocatalysis for pollutant remediation: Mini review. *J. Encapsul. Adsorpt. Sci.* **2018**, *8*, 225–255. [[CrossRef](#)]
110. Fang, G.-D.; Zhou, D.-M.; Dionysiou, D.D. Superoxide mediated production of hydroxyl radicals by magnetite nanoparticles: Demonstration in the degradation of 2-chlorobiphenyl. *J. Hazard. Mater.* **2013**, *250–251*, 68–75. [[CrossRef](#)] [[PubMed](#)]
111. Pang, Y.L.; Lim, S.; Ong, H.C.; Chong, W.T. Research progress on iron oxide-based magnetic materials: Synthesis techniques and photocatalytic applications. *Ceram. Int.* **2016**, *42*, 9–34. [[CrossRef](#)]
112. Yassin, M.T.; Al-Otibi, F.O.; Al-Askar, A.A. Photocatalytic Removal of Crystal Violet Dye Utilizing Greenly Synthesized Iron Oxide Nanoparticles. *Separations* **2023**, *10*, 513. [[CrossRef](#)]
113. Rao, A.M.; Suresh, D.; Sribalan, R.; Sandhya, G. Nano-Fe<sub>3</sub>O<sub>4</sub>-loaded chitosan salicylamide copper complex as a photocatalyst to degrade nitrophenols under the sunlight. *Appl. Phys. A* **2023**, *129*, 625. [[CrossRef](#)]
114. Kumar, A.; Sharma, G.; Naushad, M.; Thakur, S. SPION/ $\beta$ -cyclodextrin core-shell nanostructures for oil spill remediation and organic pollutant removal from waste water. *Chem. Eng. J.* **2015**, *280*, 175–187. [[CrossRef](#)]
115. Ahmad, I.; Aalam, G.; Amir, M.; Chakravarty, A.; Ali, S.W.; Ikram, S. Development of highly efficient magnetically recyclable Cu<sub>2</sub>+ /Cu<sub>0</sub> nano-photocatalyst and its enhanced catalytic performance for the degradation of organic contaminations. *Sci. Total Environ.* **2022**, *846*, 157154. [[CrossRef](#)] [[PubMed](#)]
116. Yao, H.; Fan, M.; Wang, Y.; Luo, G.; Fei, W. Magnetic titanium dioxide based nanomaterials: Synthesis, characteristics, and photocatalytic application in pollutant degradation. *J. Mater. Chem. A* **2015**, *3*, 17511–17524. [[CrossRef](#)]
117. Upadhyay, P.; Moholkar, V.S.; Chakma, S. Chapter 9—Magnetic nanomaterials-based photocatalyst for wastewater treatment. In *Handbook of Nanomaterials for Wastewater Treatment*; Bhanvase, B., Sonawane, S., Pawade, V., Pandit, A., Eds.; Elsevier: Amsterdam, The Netherlands, 2021; pp. 241–276.
118. Gopalan Sibi, M.; Verma, D.; Kim, J. Magnetic core-shell nanocatalysts: Promising versatile catalysts for organic and photocatalytic reactions. *Catal. Rev. Sci. Eng.* **2020**, *62*, 163–311. [[CrossRef](#)]
119. Sharma, R.K.; Solanki, K.; Dixit, R.; Sharma, S.; Dutta, S. Nanoengineered iron oxide-based sorbents for separation of various water pollutants: Current status, opportunities and future outlook. *Environ. Sci. Water Res. Technol.* **2021**, *7*, 818–860. [[CrossRef](#)]
120. Gopinath, K.P.; Madhav, N.V.; Krishnan, A.; Malolan, R.; Rangarajan, G. Present applications of titanium dioxide for the photocatalytic removal of pollutants from water: A review. *J. Environ. Manag.* **2020**, *270*, 110906. [[CrossRef](#)] [[PubMed](#)]
121. Jiang, J.; Pi, J.; Cai, J. The Advancing of Zinc Oxide Nanoparticles for Biomedical Applications. *Bioinorg. Chem. Appl.* **2018**, *2018*, 1062562. [[CrossRef](#)]
122. Mohammed, L.; Gomaa, H.G.; Ragab, D.; Zhu, J. Magnetic nanoparticles for environmental and biomedical applications: A review. *Particuology* **2017**, *30*, 1–14. [[CrossRef](#)]
123. Zhu, M.; Diao, G. Review on the progress in synthesis and application of magnetic carbon nanocomposites. *Nanoscale* **2011**, *3*, 2748–2767. [[CrossRef](#)]
124. Esfahani, M.R.; Aktij, S.A.; Dabaghian, Z.; Firouzjaei, M.D.; Rahimpour, A.; Eke, J.; Escobar, I.C.; Abolhassani, M.; Greenlee, L.F.; Esfahani, A.R. Nanocomposite membranes for water separation and purification: Fabrication, modification, and applications. *Sep. Purif. Technol.* **2019**, *213*, 465–499. [[CrossRef](#)]
125. Mehrnia, M.R.; Homayoonfal, M. Fouling mitigation behavior of magnetic responsive nanocomposite membranes in a magnetic membrane bioreactor. *J. Membr. Sci.* **2016**, *520*, 881–894. [[CrossRef](#)]
126. Koyuncu, I.; Gul, B.Y.; Esmaili, M.S.; Pekgenc, E.; Teber, O.O.; Tuncay, G.; Karimi, H.; Parvaz, S.; Maleki, A.; Vatanpour, V. Modification of PVDF membranes by incorporation Fe<sub>3</sub>O<sub>4</sub>@ Xanthan gum to improve anti-fouling, anti-bacterial, and separation performance. *J. Environ. Chem. Eng.* **2022**, *10*, 107784. [[CrossRef](#)]
127. Huang, Y.; Xiao, C.-F.; Huang, Q.-L.; Liu, H.-L.; Hao, J.-Q.; Song, L. Magnetic field induced orderly arrangement of Fe<sub>3</sub>O<sub>4</sub>/GO composite particles for preparation of Fe<sub>3</sub>O<sub>4</sub>/GO/PVDF membrane. *J. Membr. Sci.* **2018**, *548*, 184–193. [[CrossRef](#)]
128. Tang, J.; Yuan, W.; Wang, J.; Tang, J.; Li, H.; Zhang, Y. Perfluorosulfonate ionomer membranes with improved through-plane proton conductivity fabricated under magnetic field. *J. Membr. Sci.* **2012**, *423*, 267–274. [[CrossRef](#)]

129. Bhaduri, B.; Dixit, A.K.; Tripathi, K.M. Magnetic Nanoparticles: Application in the Removal of Next-Generation Pollutants from Wastewater. In *New Trends in Emerging Environmental Contaminants*; Singh, P., Agarwal, A.K., Gupta Maliyekkal, S.M., Eds.; Springer: Singapore, 2022; pp. 287–310.
130. Ali, I.; Tan, X.; Li, J.; Peng, C.; Wan, P.; Naz, I.; Duan, Z.; Ruan, Y. Innovations in the Development of Promising Adsorbents for the Remediation of Microplastics and Nanoplastics—A Critical Review. *Water Res.* **2022**, *230*, 119526. [[CrossRef](#)] [[PubMed](#)]
131. Yan, R.; Lin, S.; Jiang, W.; Yu, X.; Zhang, L.; Zhao, W.; Sui, Q. Effect of aggregation behavior on microplastic removal by magnetic Fe<sub>3</sub>O<sub>4</sub> nanoparticles. *Sci. Total Environ.* **2023**, *898*, 165431. [[CrossRef](#)]
132. Shi, X.; Zhang, X.; Gao, W.; Zhang, Y.; He, D. Removal of microplastics from water by magnetic nano-Fe<sub>3</sub>O<sub>4</sub>. *Sci. Total Environ.* **2022**, *802*, 149838. [[CrossRef](#)]
133. Miranda Zoppas, F.; Sacco, N.; Soffietti, J.; Devard, A.; Akhter, F.; Marchesini, F.A. Catalytic approaches for the removal of microplastics from water: Recent advances and future opportunities. *Chem. Eng. J. Adv.* **2023**, *16*, 100529. [[CrossRef](#)]
134. Staroń, P.; Kuciakowski, J.; Chwastowski, J. Biocomposite of hydrochar and *Lindnera jadinii* with magnetic properties for adsorptive removal of cadmium ions. *J. Environ. Chem. Eng.* **2023**, *11*, 110270. [[CrossRef](#)]
135. Hou, M.; Wang, Z.; Zhang, J.; Yang, Y.; Li, Y.; Sun, T.; Luo, H.; Wan, J.; Chen, K. Fabrication of polyethyleneimine functionalized magnetite nanoparticles for recyclable recovery of fucoidan from aqueous solution. *Colloids Surf. B* **2023**, *229*, 113478. [[CrossRef](#)]
136. Zheng, W.; Sun, Y.; Gu, Y. Assembly of UiO-66 onto Co-doped Fe<sub>3</sub>O<sub>4</sub> nanoparticles to activate peroxymonosulfate for efficient degradation of fenitrothion and simultaneous in-situ adsorption of released phosphate. *J. Hazard. Mater.* **2022**, *436*, 129058. [[CrossRef](#)]
137. Liu, F.; Hu, J.; Hu, B. Magnetic MXene-NH<sub>2</sub> decorated with persimmon tannin for highly efficient elimination of U (VI) and Cr (VI) from aquatic environment. *Int. J. Biol. Macromol.* **2022**, *219*, 886–896. [[CrossRef](#)] [[PubMed](#)]
138. Taşçı, S.; Özgüven, A.; Yıldız, B. Multi-response/multi-step optimization of heterogeneous Fenton process with Fe<sub>3</sub>O<sub>4</sub> catalyst for the treatment of landfill leachate. *Water Air Soil. Pollut.* **2021**, *232*, 275. [[CrossRef](#)]
139. Akbas, Y.A.; Yusan, S.; Sert, S.; Aytas, S. Sorption of Ce (III) on magnetic/olive pomace nanocomposite: Isotherm, kinetic and thermodynamic studies. *Environ. Sci. Pollut. Res.* **2021**, *28*, 56782–56794. [[CrossRef](#)] [[PubMed](#)]
140. Mateus, G.A.P.; Dos Santos, T.R.T.; Sanches, I.S.; Silva, M.F.; de Andrade, M.B.; Paludo, M.P.; Gomes, R.G.; Bergamasco, R. Evaluation of a magnetic coagulant based on Fe<sub>3</sub>O<sub>4</sub> nanoparticles and *Moringa oleifera* extract on tartrazine removal: Coagulation-adsorption and kinetics studies. *Environ. Technol.* **2020**, *41*, 1648–1663. [[CrossRef](#)]
141. Lei, C.; Wang, C.; Chen, W.; He, M.; Huang, B. Polyaniline@ magnetic chitosan nanomaterials for highly efficient simultaneous adsorption and in-situ chemical reduction of hexavalent chromium: Removal efficacy and mechanisms. *Sci. Total Environ.* **2020**, *733*, 139316. [[CrossRef](#)]
142. Li, Y.; Zhang, H.; Chen, Y.; Huang, L.; Lin, Z.; Cai, Z. Core-shell structured magnetic covalent organic framework nanocomposites for triclosan and triclocarban adsorption. *ACS Appl. Mater. Interfaces* **2019**, *11*, 22492–22500. [[CrossRef](#)]
143. Li, Q.; Kong, H.; Li, P.; Shao, J.; He, Y. Photo-Fenton degradation of amoxicillin via magnetic TiO<sub>2</sub>-graphene oxide-Fe<sub>3</sub>O<sub>4</sub> composite with a submerged magnetic separation membrane photocatalytic reactor (SMSMPR). *J. Hazard. Mater.* **2019**, *373*, 437–446. [[CrossRef](#)]

**Disclaimer/Publisher’s Note:** The statements, opinions and data contained in all publications are solely those of the individual author(s) and contributor(s) and not of MDPI and/or the editor(s). MDPI and/or the editor(s) disclaim responsibility for any injury to people or property resulting from any ideas, methods, instructions or products referred to in the content.